Published in final edited form as:

Clin Pharmacol Ther. 2018 November ; 104(5): 865–889. doi:10.1002/cpt.1183.

Advancing Predictions of Tissue and Intracellular Drug Concentrations Using *In Vitro*, Imaging and PBPK Modeling Approaches

Yingying Guo[1], **Xiaoyan Chu**[2], **Neil J. Parrott**[3], **Kim L.R. Brouwer**[4], **Vicky Hsu**[5], **Swati Nagar**[6], **Pär Matsson**[7], **Pradeep Sharma**[8], **Jan Snoeys**[9], **Yuichi Sugiyama**[10], **Daniel Tatosian**[11], **Jashvant D. Unadkat**[12], **Shiew-Mei Huang**[5], and **Aleksandra Galetin**[13,*] **on behalf of the International Transporter Consortium**

Yingying Guo: guo_yingying@lilly.com; Xiaoyan Chu: xiaoyan_chu@merck.com; Neil J. Parrott: neil_john.parrott@roche.com; Kim L.R. Brouwer: kbrouwer@unc.edu; Vicky Hsu: Vicky.Hsu@fda.hhs.gov; Swati Nagar: swati.nagar@temple.edu; Pär Matsson: par.matsson@farmaci.uu.se; Pradeep Sharma: Pradeep.Sharma@astrazeneca.com; Jan Snoeys: jsnoeys@its.jnj.com; Yuichi Sugiyama: ychi.sugiyama@riken.jp; Daniel Tatosian: daniel_tatosian@merck.com; Jashvant D. Unadkat: jash@uw.edu; Shiew-Mei Huang: shiewmei.huang@fda.hhs.gov; Aleksandra Galetin: aleksandra.galetin@manchester.ac.uk

[1]Investigational Drug Disposition, Eli Lilly and Company, Lilly Corporate Center, DC0714, Indianapolis, IN 46285, USA; Tel: 317-277-4324 [2]Department of Pharmacokinetics, Pharmacodynamics and Drug Metabolism, Merck & Co., Inc., Kenilworth, New Jersey 07033, USA; 732-594-0977 [3]Pharmaceutical Sciences, Pharmaceutical Research and Early Development, Roche Innovation Centre Basel, F. Hoffmann-La Roche Ltd., Grenzacherstrasse 124, CH-4070 Basel, Switzerland [4]Division of Pharmacotherapy and Experimental Therapeutics, UNC Eshelman School of Pharmacy, The University of North Carolina at Chapel Hill, CB #7569 Kerr Hall, Chapel Hill, NC 27599-7569, USA; Tel: (919) 962-7030 [5]Office of Clinical Pharmacology, Office of Translational Sciences, Center for Drug Evaluation and Research, US Food and Drug Administration, 10903 New Hampshire Ave, Silver Spring, MD 20993, USA;

[*]Corresponding author: Dr Aleksandra Galetin, Centre for Applied Pharmacokinetic Research, School of Health Sciences, The University of Manchester, Stopford Building, Oxford Road, Manchester, M13 9PT, UK, Tel: (+) 44 161 275 6886; Aleksandra.Galetin@manchester.ac.uk.

Collaborators: Eef Hoeben Quantitative Sciences, Janssen R&D, Beerse, Belgium

Dapeng Chen, Department of Pharmacokinetics, Pharmacodynamics and Drug Metabolism, Merck & Co., Inc., Boston, MA 02115, USA

Georgy Hartmann, Department of Pharmacokinetics, Pharmacodynamics and Drug Metabolism, Merck & Co., Inc., Kenilworth, NJ 07033, USA

Karsten Menzel, Department of Pharmacokinetics, Pharmacodynamics and Drug Metabolism, Merck & Co., Inc., West Point, PA 19486, USA

Supplemental Material - Table S1ab, Table S2, Table S3, Table S4, Table S5ab, Figure S1, Figure S2
Supplemental Reading List

This white paper is based on the session held at the 3rd International Transporter Consortium (ITC) Workshop – Transporters in Drug Development ASCPT Pre-conference, 13–14th March 2017.

Conflict of interest: KLRB is a co-inventor of the sandwich-cultured hepatocyte technology for quantification of biliary excretion (B-CLEAR®) and related technologies, which have been licensed exclusively to Qualyst Transporter Solutions, LLC. Y.G. is an employee and stockholder of Eli Lilly and Company. D.A.T. and X.C. are employees and stockholders of Merck & Co., Inc.. P.S. is an employee and stockholder of AstraZeneca. J.S. is employee of Janssen and may own stock options in the company. The contents of this article reflect the views of the authors and should not be construed to represent the views or policies of the FDA or the National Institutes of Health. No official support or endorsement by the FDA is intended or should be inferred. The mention of commercial products, their sources, or their use in connection with material reported herein is not to be construed as either an actual or implied endorsement of such products by the FDA. S.-M.H., an Associate Editor of *Clinical Pharmacology & Therapeutics*, was not involved in the review or decision process for this article.

301-796-1541 [6]Temple University School of Pharmacy, Department of Pharmaceutical Sciences, 3307 N Broad Street, Philadelphia PA 19140, USA; 215-707-9110 [7]Department of Pharmacy, Uppsala University, Box 580, SE-75123 Uppsala, Sweden +46-(0)18-471 46 30 [8]Safety and ADME Translational Sciences, Drug Safety and Metabolism, IMED Biotech Unit, AstraZeneca R&D, Cambridge CB4 0WG, UK [9]Department of Pharmacokinetics, Dynamics and Metabolism, Janssen R&D, Beerse, Belgium; Tel: +32-14606812 [10]Sugiyama Laboratory, RIKEN Innovation Center, RIKEN Research Cluster for Innovation, Yokohama 230-0045, Japan; Tel: (045) 506-1814 [11]Department of Pharmacokinetics, Pharmacodynamics and Drug Metabolism, Merck & Co., Inc., Kenilworth, New Jersey 07033, USA; 908-464-2375 [12]Department of Pharmaceutics, University of Washington, Seattle, WA, USA; 206-685-2869 [13]Centre for Applied Pharmacokinetic Research, School of Health Sciences, The University of Manchester, Manchester M13 9PT, UK; + 44-161-275-6886

Abstract

This white paper examines recent progress, applications and challenges in predicting unbound and total tissue and intra/subcellular drug concentrations using *in vitro* and preclinical models, imaging techniques and physiologically-based pharmacokinetic (PBPK) modeling. Published examples, regulatory submissions and case studies illustrate the application of different types of data in drug development to support modeling and decision making for compounds with transporter-mediated disposition, and likely disconnects between tissue and systemic drug exposure. The goals of this manuscript are to illustrate current best practices and outline practical strategies for selecting appropriate *in vitro* and *in vivo* experimental methods to estimate or predict tissue and plasma concentrations, and to use these data in the application of PBPK modeling for human PK, efficacy and safety assessment in drug development.

Keywords

Physiology-based pharmacokinetics; Transporters; In Vitro; Imaging; In-vitro in-vivo correlation; Drug Development; Drug Transport; Drug-Drug Interactions; Distribution

---

Knowledge of unbound tissue drug concentrations is critical to the understanding of efficacy, toxicity and drug-drug interactions (DDI) (1). Use of local interstitial concentrations to predict receptor occupancy at the target tissue should improve decision making for candidate molecules that meet the desired pharmacokinetic (PK) and pharmacodynamic (PD) profile. For highly-permeable drugs interacting with plasma membrane receptor(s), the unbound concentration at the site of action is assumed to be equal to the blood or plasma unbound drug concentrations. However, when intracellular and subcellular targets are of interest, this assumption may not be valid, especially for drugs with transporter-mediated disposition, as the activity of transporters at the tissue-blood barrier can result in “asymmetry” between the tissue and blood unbound drug concentrations (2). Transporter-mediated drug disposition often entails the complex interplay of multiple processes and defining the rate determining step and outcome of these multiple factors is a challenge (1, 3–5). As a result, profound DDIs can occur at the tissue level which cannot be discerned in a typical clinical DDI study

where only the systemic concentrations of the substrate drug are measured. For example, changes in liver (metformin) and brain (verapamil) concentrations in the presence of a transporter inhibitor, which may have consequences on projected drug efficacy and safety, may not be reflected in changes in plasma exposure (6, 7). The opposite can occur where a profound DDI is observed in terms of changes in systemic concentrations, but without impacting tissue drug exposure (e.g., no change in statin efficacy as a result of OATP1B1 polymorphism) (3). Furthermore, subcellular drug accumulation can result in toxicity, as illustrated by fialuridine where a mitochondrial-membrane transporter is associated with drug-induced liver injury (8). The extended clearance model defines the fundamental principles to describe the interplay between passive diffusion, transporter-mediated clearances and metabolism, which together with intracellular binding determine tissue drug concentration (4, 5, 9, 10). The consequences of inhibition of certain transporter processes on liver exposure will vary depending on the rate-determining step(s) of drug clearance and whether liver is the predominant eliminating organ (Figure 1), or if there is also a significant non-hepatic contribution to the elimination (Figure S1).

Physiologically-based pharmacokinetic (PBPK) modeling is a key translational tool that allows mechanistic evaluation of the interplay of all processes governing drug distribution and clearance, and simulation of both systemic and tissue exposure as a result of changes in enzyme and/or transporter activity (1, 10, 11). The increased use of PBPK modeling in drug development is reflected in the number and diversity of examples reported in the literature and in regulatory submissions summarized here, together with recently published DDI and PBPK guidance documents from regulatory agencies and ongoing discussions on PBPK model verification/qualification (http://www.ema.europa.eu/docs/en_GB/document_library/Scientific_guideline/2016/07/WC500211315.pdf; https://www.fda.gov/Drugs/GuidanceComplianceRegulatoryInformation/Guidances/ucm064982.htm). Application of *in vitro-in vivo* extrapolation (IVIVE) for transporter-mediated disposition in PBPK models requires kinetic determinations of transport processes in well-defined cellular systems and knowledge of the transporter expression *in vitro* in relation to *in vivo*. The best practices for selection of *in vitro* systems, data analyses for acquiring transporter kinetics, and the most commonly used principles in transporter IVIVE have been summarized previously (10). Recent progress in translation of transporter-mediated PK, including also specific populations (organ impairment, disease), will be discussed in the sections below. Routine verification of PBPK-based tissue predictions is not possible in humans, and the best approach to circumvent this limitation is to verify predicted tissue drug concentrations for selected model substrates that can interrogate the transporters of interest. Such verification is possible with non-invasive imaging such as positron emission tomography (PET), single-photon emission CT (SPECT), magnetic resonance imaging (MRI), or the more invasive method, microdialysis (2).

Focusing on the progress since publication by Chu et al. (2), this whitepaper highlights advantages and limitations of *in vitro*/preclinical models, imaging methods and PBPK modeling as tools to estimate or predict intracellular drug concentrations and potential differences between tissue and systemic exposure in case of transporter-mediated disposition. Integration of different approaches is illustrated by selected published examples, regulatory submissions, industrial case studies and a proposed workflow. Opportunities and

recommendations for future directions are discussed with a focus on refining translational modeling of transporter-mediated PK and DDIs.

IN VITRO METHODS FOR ESTIMATION OF INTRACELLULAR/ SUBCELLULAR DRUG CONCENTRATIONS

In vitro systems are important tools in analyzing determinants of intracellular/subcellular drug disposition and establishing appropriate parameters for transporter IVIVE (2, 10). *In vitro* studies also provide estimates for crucial parameters such as fraction unbound in cell ($f_{u,cell}$) and steady-state unbound tissue-to-blood partition coefficient ($K_{p,uu}$) that can be used as inputs in mechanistic modeling. As detailed previously (2, 3) and conceptually illustrated in Figure 1, $K_{p,uu}$ reflects the complex interplay of multiple processes governing unbound tissue drug concentrations. This section provides a critical overview of *in vitro* methods to determine intracellular and subcellular drug concentrations, with a focus on the recent progress in determining $K_{p,uu}$. In addition, application of transporter expression data in proteomic-informed transporter IVIVE is illustrated.

Most drug accumulation assays measure total cellular drug concentrations, which represents the sum of drug accessible to the cytosol, drug bound to cellular membranes and macromolecules, and drug that is distributed to subcellular organelle compartments including lysosomes, mitochondria and nuclei. Current methods to determine *in vitro* $K_{p,uu}$ and estimate cellular drug binding can be divided into five categories (details in Table 1): i) Binding Method to directly measure binding to cell or tissue homogenate (12–15); ii) Temperature Method to calculate binding from total cellular drug accumulation at 37°C and 4°C (16, 17); iii) Structure-based Prediction Method to estimate binding from molecular properties by structure-property relationship models (12, 18); iv) Kinetic Modeling Method to derive binding by fitting mechanistic models to drug accumulation data (18); and v) Extended Clearance Model (ECM) Method to calculate $K_{p,uu}$ based on transporter kinetic parameters derived from *in vitro* assays (15, 17). Each method is associated with specific assumptions that should be considered when comparing results and selecting the most suitable approach for a particular application.

Binding Method—Total cell to medium concentration ratio (K_p), $f_{u,cell}$ or fraction unbound in tissue (e.g., $f_{u,liver}$) and fraction unbound in medium ($f_{u,medium}$) are individually measured and combined to derive the $K_{p,uu}$ value (Table 1). Binding may be determined using equilibrium dialysis of cell or tissue homogenate. By accounting for the dilution of homogenate in the assay, $f_{u,cell}$ or $f_{u,liver}$ can be calculated. The method thus represents a comparatively direct measurement of cellular drug binding with a central assumption that binding is not altered by the homogenization procedure. Non-saturation of binding for a chemically diverse set of compounds, along with the nature of the molecular properties most strongly associated with binding (high lipophilicity, small cross-sectional area, and a preference for positive molecular charge) suggests that partitioning to phospholipid membranes is a major contributor to cell binding (12). However, binding equilibrium between cellular compartments may shift in homogenized *vs.* live cells, different dilution factors which impact cell density may be used for homogenized cells/tissues (19), incubation

media may differ regarding albumin content (20), and depending on the homogenization procedures (2), intracellular organelle membranes may or may not be disrupted. These factors may have contributed to some contradictory findings in $f_{u,cell}$ values between laboratories discussed below.

Temperature Method—Instead of combining two distinct assays for $f_{u,cell}$ and K_p as in the Binding Method, $K_{p,uu}$ is determined by measuring steady-state medium and cell concentration with the same method, but at two different temperatures: 37°C and 4°C (16) (Table 1). The estimation of $f_{u,cell}$ is based on the steady-state uptake at 4°C. Important assumptions underlying this method are that tissue binding does not involve temperature- or energy-dependent processes (e.g., transporter-mediated flux, metabolism, and ion gradients that might shift cellular equilibria when non-functional at 4°C). However, the impact of temperature on tissue binding, membrane potential and fluidity are not well established. In addition, disadvantages associated with disruption and release of organelle proteins remain. Initial studies have indicated certain temperature dependence of binding and tissue permeability (15, 17, 21), but this needs to be confirmed with large, chemically diverse datasets.

Structure-based Prediction Method—Initial studies in suspended rat hepatocytes showed a correlation between $Logf_{u,cell}$ and $LogD_{7.4}$ for 13 anionic transporter substrates (18). The correlation of anionic drugs was later extended to plated (22) and suspended human hepatocytes (15). $LogD_{7.4}$ was also an important predictor of $f_{u,cell}$, along with additional molecular properties (charge and steric descriptors putatively describing interactions with cellular membranes) for a larger set of anionic, cationic and neutral drugs (12). The $f_{u,cell}$ estimated based on physicochemical properties has been further utilized to calculate $K_{p,uu}$ (Table 1). Since either Binding or Temperature Methods were used to derive initial experimental data, the associated limitations have been carried over (Table 1).

Kinetic Modeling Method—This method uses mathematical modeling to derive $K_{p,uu}$ estimates from cellular drug accumulation experiments. For example, the initial drug uptake rate was measured in suspended hepatocytes in the presence of a nonspecific cytochrome P450 inhibitor (18). Kinetic parameters including active uptake V_{max}, K_m, and passive diffusion were obtained simultaneously to calculate $K_{p,uu}$ (Table 1), using a reduced form of the extended clearance equation. The method assumes knowledge of the mechanisms involved in cellular drug disposition, and may lead to overestimation of the true $K_{p,uu}$ for the following reasons: 1) the system does not consider the influence of efflux transporters, biliary excretion or unaccounted non-CYP mediated metabolism), 2) active influx clearance is calculated based on the initial uptake rate, which may include drug transport mediated by both facilitated diffusion transporters and active transporters, and 3) the passive influx diffusion permeation is assumed to be equal to the passive efflux diffusion permeation; this may not always be true, for example in the case of anions (17).

Extended Clearance Model (ECM) Method—Steady-state $K_{p,uu}$ can be described using the extended clearance equation incorporating the individual processes involved in *in vitro* hepatic clearances (15, 17). The fundamental difference from the above-mentioned

Kinetic Modeling method is that the impact of compound disappearance via sinusoidal efflux, biliary excretion, and metabolism is explicitly considered. One limitation is that *in vitro-in vivo* correlation (IVIVC) for the parameters used to calculate $K_{p,uu}$ has not been fully validated. As in the Kinetic Modeling method, accurate predictions rely on knowledge of relevant drug disposition mechanisms and their adequate parameterization. In both the Kinetic Modeling method and ECM method, binding is not addressed explicitly, and can be calculated from the model-based $K_{p,uu}$ if combined with a K_p measurement in the same system. However, errors in estimating parameters contributing to $K_{p,uu}$ would propagate to calculation of $f_{u,cell}$.

Overall, the Kinetic Modeling method and ECM method rely on assumptions that the relevant cellular processes are known and respective parameters can be accurately determined. These methods require rich datasets generated by laborious experimental processes in order to minimize uncertainty in parameter estimates. In contrast, the Structure-based Prediction Method may provide an initial $f_{u,cell}$ estimate in the absence of *in vitro* data if the compound properties are within the physicochemical space of compounds in the training set used to define the relationship with $f_{u,cell}$. The Binding and Temperature methods are more agnostic regarding the processes involved compared to the Kinetic Modeling method and ECM method, while at the same time less mechanistically informative.

Estimation of Subcellular Drug Concentrations—To fully understand the factors determining drug cellular concentrations it is important to consider subcellular drug distribution. Drug molecules may distribute preferentially to various subcellular organelles even without transporter effects, due to the electrochemical and pH gradients across membranes and interactions driven by compound lipophilicity, charge, and ionization potential. The subcellular accumulation of lipophilic bases may impact $K_{p,uu}$ (15, 23). Indirect experimental methodologies used for estimation of subcellular drug concentrations have been discussed previously (2, 23, 24). Recent examples in combining experimental approaches with mechanistic modeling to predict subcellular drug concentrations are highlighted here.

Lysosomal sequestration may be an important contributor to the accumulation of drugs that are lipophilic (LogP>1) and amphiphilic with ionizable amines (pKa>6) in lysosome-rich cells such as Kupffer cells, and alveolar macrophages. The extent of lysosomal sequestration can be determined by measuring drug concentrations in cultured cells using indirect methods that abolish the lysosome-cytosol pH gradient, e.g., ammonium chloride (NH_4Cl) (23) or chloroquine (12). Of note, modulating the pH gradient affects both total cell-to-unbound medium concentration ratio ($K_{p,u}$) and $K_{p,uu}$. Alternatively, cellular accumulation can be measured at low and high drug concentrations, assuming that saturable cellular uptake at a low drug concentration is driven by lysosomal sequestration rather than a transporter-mediated process. Lysosomal sequestration may change accumulation kinetics, as observed with the altered uptake rate of clarithromycin in the presence of NH_4Cl in the macrophage cell line NR8383 (23). Indirect experimental methods do not account for the impact on drug binding to membranes due to changes in ionic strength and membrane surface potential at higher drug concentrations. Lysosomal drug concentrations can be directly measured by

isolating lysosomes with novel techniques using magnetic nanoparticles (25); evaluation of this method is in progress.

Previously, generic in silico cell models were proposed to describe the dynamics of drug accumulation in lysosomes (26). Recently, these models were refined and adapted to specific cell types (e.g., macrophages) accounting for pH gradients and electrochemical potentials across cell and organelle membranes to simulate drug concentrations in cytosol, lysosomes and mitochondria. Membrane partitioning either predicted from phospholipid membrane composition data or measured by indirect methods was incorporated into models to predict lysosomotropic properties of respiratory drugs (27). The application of this mechanistic cellular model to predict lysosomal drug concentrations needs further evaluation with larger basic drug datasets and extension of the model to other cell types (e.g., hepatocytes) where lysosomotropic drugs may accumulate and induce phospholipidosis. Recently, an extended mechanistic tissue-composition based model accounting for lysosomal sequestration was proposed and evaluated using a dataset of 28 basic drugs. Differences in cytosolic and lysosomal pH and in lysosomal volume fractions of the individual cell types/tissues were implemented in the model. Consideration of lysosomal sequestration moderately improved the accuracy of $K_{p,u}$ predictions (up to 3-fold change) for lysosome-rich tissues. This result is not entirely surprising as the fraction of lysosome-rich cells (e.g., Kupffer cells) is generally low (<5%) in tissues (28).

Positively charged drug molecules may be trapped in mitochondria as a result of the negative transmembrane electrical potential relative to the cytosol. A mechanistic model accounting for pH and electrochemical potentials across plasma and organelle membranes (including mitochondria) and permeability of both ionized and neutral species explained reasonably the observed $K_{p,uu}$ for multiple tissues in rats treated with investigational drugs (e.g., hepatoselective glucokinase activators) (29). Utilizing a similar approach and additional incorporation of a bi-directional, saturable effect on the ionized permeability to characterize transporter uptake kinetics, metformin subcellular concentrations, including mitochondria, were predicted in stably transfected human embryonic kidney 293 (HEK293) cells (30).

Method comparison and qualification

Comparison of Cellular Systems—Various *in vitro* cellular systems have been used to determine *in vitro* $K_{p,uu}$ and estimate cellular drug binding (Table 1), and the associated advantages and limitations are summarized below. Most methods have focused on suspended hepatocytes, except for the Binding Method which uses multiple cell systems. In principle, the above-mentioned fundamental approaches can be applied for diverse primary cell types to estimate unbound drug concentrations in various human tissues. These predicted regional exposures can then be correlated with efficacy and/or safety endpoints, as illustrated in the Table S1a for brain $K_{p,uu}$.

Cell lines such as HEK293 (12) and HeLa (31) are most commonly used as hosts to express membrane transporters or proteins that are therapeutic drug targets. These cell systems are relatively deficient in baseline drug transport/metabolic activities, but may be used in multi-well formats and optimized into high-throughput tools for exploring $K_{p,uu}$ during early drug discovery. However, the intracellular architecture of these cell lines does not exactly mimic

native human primary cell systems and reproducibility of $K_{p,uu}$ estimates from different cell passages has not been reported.

$K_{p,uu}$ has been determined in different formats of primary hepatocytes, namely suspended and plated hepatocytes (14, 17, 18, 32), as well as sandwich-cultured hepatocytes (SCH) (13, 33). Culture conditions have been shown to affect the expression and activity of uptake and efflux transporters, as well as drug-metabolizing enzymes, which should be considered when comparing $K_{p,uu}$ results. For instance, suspended hepatocytes (fresh rat and cryopreserved human hepatocytes) are known to exhibit passive, active uptake and metabolic activity, but not efflux, which is captured in SCH. Determination of $K_{p,uu}$ in SCH may be useful when attempting to correlate unbound intracellular drug concentrations with endpoints including 1) efflux clearance, 2) hepatotoxicity potentially due to perturbation of hepatic efflux transporters, 3) drug efficacy when the target protein is intracellularly located, and 4) DDI predictions due to inhibition of metabolism and efflux transporters (34). Although a good correlation was observed between $K_{p,uu}$ in rat SCH and *in situ* rat liver perfusion systems for selected compounds (13), a recent study reported that rat SCH $K_{p,uu}$ estimates were lower compared to data from suspended or plated hepatocytes (33).

Brain homogenates and slices (2) from preclinical species are commonly utilized for estimating tissue $K_{p,uu}$. Brain slices may be more physiologically relevant than brain homogenates because of intact cell-cell interactions, retention of pH gradients and active transport systems (Table S1b). However, due to the absence of the blood-brain barrier, brain slices are not an appropriate model to evaluate permeability across the blood-brain barrier and the role of efflux transporters.

$K_{p,uu}$ and $f_{u,cell}$ Comparisons—Side-by-side comparisons of different $K_{p,uu}$ *and* $f_{u,cell}$ methodologies are rare to date, and published datasets include only partially overlapping compounds. The intracellular binding of model drugs measured by the Binding Method has shown high correlation between values obtained in the HEK293 cell line, human or rat hepatocytes (12, 19) and brain tissue (35); differences in lipid and/or protein content were suggested to account for differing binding capacity between cell and tissue types. Rat $f_{u,liver}$ was proposed as a potential surrogate for liver binding in other species, including human, in early drug discovery based on data from 22 structurally diverse compounds (19). A recent analysis (17) reported that the model-based estimates were typically higher and more sensitive to inter-batch variability than the temperature-based estimates. In a comprehensive comparison of the $f_{u,cell}$ values between three methods (the Binding, Temperature and Structure-based Prediction Methods), Riede et al. (15) noted a consistently lower unbound fraction using the Binding Method, with half of the 18 compounds exhibiting differences greater than 10-fold between the methods. However, such a trend is not consistent with data obtained by the Binding Method in other laboratories (Figure S2A). A comparison of literature reported $f_{u,cell}$ values for the seven compounds for which data were available for all three major methods is shown in Figure S2B. Excluding the Riede et al. Binding Method-based $f_{u,cell}$ data (15), which were consistently lower than the other reports (19-fold on average), all the other data were within 1–6-fold of the per-compound average (mean: 1.9-fold). Thus, for this limited dataset the three major methods appear to provide consistent information about cellular drug binding.

In general, the *in vitro* $K_{p,uu}$ data generated from different methods (Table S2) varied with the exception of a close correlation between values obtained by the Binding Method and the ECM method for 11/18 compounds. The Structure-based Prediction and Temperature Methods trended higher in most of the same 18 compounds compared to the ECM method, although the Temperature Method has shown better correlation with the ECM method for compounds with certain characteristics, i.e., ECM class 2/4 and 1/3 with low intrinsic clearance (15). The Kinetic Modeling Method also generated higher *in vitro* $K_{p,uu}$ values than the ECM method for three statins, but consideration of inside-negative membrane potential resulted in a closer agreement with ECM (17). In summary, comparisons of different $K_{p,uu}$ *and* $f_{u,cell}$ methodologies are currently based on limited datasets, and need to be extended to compounds with more diverse chemistry structures and drug disposition pathways.

In Vitro-In Vivo Correlation (IVIVC) of In Vitro $K_{p,uu}$ Data—Rich target-site data collected in preclinical species allowed the development and refinement of comprehensive models to predict *in vivo* $K_{p,uu}$ and understand IVIVC of *in vitro* $K_{p,uu}$. Rat and monkey IVIVC studies exemplify this use of preclinical data as a proof-of-concept (Table S2). Examples of successful within-species IVIVC have been published recently, as illustrated for rosuvastatin and pravastatin (14). Although promising, this approach needs to be validated, replicated and examined further using a large diverse group of compounds including those with extensive metabolism. Another study reported that ECM-derived *in vitro* $K_{p,uu}$ combined with intrahepatic concentrations and BSEP inhibition data predicted clinical drug-induced cholestasis for 17/18 compounds (36). However, opinions differed concerning categorization of the cholestasis class for some of the compounds investigated (36, 37). In addition, preclinical whole organ perfusion studies have been used to develop predictive models for unbound intracellular concentrations (21) and knockout and human transporter ‘knock-in’ rodent models continue to aid mechanistic understanding of the role of respective transporter(s) (38, 39). Several recent examples of experimental and modeling advances in brain $K_{p,uu}$ determination and prediction in mouse, rat, and monkey are listed in Tables S1a and S1b. Direct scaling of preclinical results to human may not be feasible given the known and possibly as yet unknown differences in transporter protein expression/activity across species (40).

Proteomics-informed transporter in vitro-in vivo extrapolation (IVIVE)

Consideration of differences in the transporter activity/expression between *in vitro* systems and *in vivo* is an important factor for the prediction of transporter-mediated clearance. Progress to date has been limited for the relative activity factor (RAF) approach (41) due to the lack of availability of selective *in vitro/in vivo* transporter probe substrates. In contrast, more advances have been made in quantitative proteomics informing the relative expression factor (REF) (42, 43), as illustrated by prediction of transporter-mediated clearance of drugs from data obtained in HEK cells individually expressing the relevant transporters (44, 45). Multiple studies have quantitatively analyzed cellular systems and tissues by mass spectrometry for total transporter abundance in brain, liver, intestine, kidney, lung, as well as hepatic uptake transporter expression in the plasma membrane (See supplemental reading list for more information). Recent meta-analysis of reported OATP abundance data in plated

and sandwich-cultured hepatocytes and liver showed that the mean abundance of hepatic uptake transporters, except for OATP2B1, did not differ significantly between cryopreserved human hepatocytes and liver tissue (42), while another study indicated significantly lower transporter expression in freshly isolated human hepatocytes relative to human liver from the same donors (45). Most of the proteomic studies do not provide corresponding pharmacogenomic or functional activity data to allow delineation of the true inter-individual variability and experimental/technical variability; the latter may result from choices of standard peptides (46), sample preparations or the proteomic methodology/membrane isolation and fractionation (47). While the majority of transporter IVIVE studies have focused on hepatic effects, transporters expressed in other tissues have also been investigated. For some renal transporters (e.g., OAT3), IVIVE was successful by applying directly the *in vitro*-derived transporter data to predict *in vivo* disposition (48), whereas in other instances optimization of transporter activity/expression was performed using clinical data to bridge the gap between *in vitro* extrapolation and the actual observation (49–51).

It is evident that expression data alone may not explain the under-prediction of transporter-mediated clearance and need for compound-dependent scaling factors. But the use of transporter abundance data in IVIVE offers added value by allowing rational incorporation of inter-individual variability, which enables characterization of different populations (52, 53). Considering existing methodological differences, even when the same biological samples are analyzed (47), it would be prudent to apply the same proteomic methodology for the analysis of cellular and tissue samples when possible. Additional studies that provide abundance-functional activity correlations are needed to profile enzymes and transporter expression of more diverse tissues/disease states and larger sample sizes. This information would allow for incorporation of population variability and increase confidence in the use proteomic data in PBPK modeling.

IMAGING METHODS FOR MEASURING DRUG CONCENTRATIONS IN TISSUES

PET

Nuclear imaging techniques, such as PET and SPECT, involve administration of a radiolabeled drug of interest and non-invasively measuring tissue drug concentrations in 3-dimensions (54). PET imaging utilizes drugs labeled with positron-emitting isotopes such as ^{11}C or ^{18}F that have short half-lives (~20 and 110 min, respectively). Since these isotopes can be incorporated into the structure of the drug, the tissue distribution of the drug itself, rather than its derivative/analog, can be studied. When determining tissue drug concentrations, PET provides greater spatial localization and resolution (within ~4–5 mm) than γS/SPECT (~10 mm) because the latter uses radioisotopes that emit gamma photons in only one direction. The resolution of PET imaging is sufficient to discern *in vivo* regional distribution of drugs within an organ (e.g., different parts of the brain, Table 2), but like all other imaging methods currently available, it is not sufficient to discern drug distribution at the cellular/subcellular level. The advantage of the short half-life of PET isotopes is that radiation exposure to the subject is limited and studies can be conducted in the same subject with and without transport inhibitor(s) on the same day. Due to sensitivity of PET, the

labeled drug can be administered in micro or tracer doses (picomolar to nanomolar for PET *vs.* nanomolar to micromolar for SPECT) and, therefore, pharmacological effects are avoided. If nonlinearity in tissue distribution is a concern, the PET tracer could be co-administered with pharmacological doses of the unlabeled drug (examples in Table 2). The disadvantages of PET imaging are that the synthesis of the labeled drug has to be conducted in-house immediately prior to drug administration, and PET requires a multidisciplinary team and costly equipment.

Imaging methods have the further disadvantage that they cannot distinguish between the parent drug and metabolite(s) if the metabolite(s) retain(s) the label; therefore, metabolically stable PET tracers are preferred (6, 54, 55). For drugs that are extensively metabolized and administered as tracers, tissue drug distribution must be conducted over a period of time when the metabolism of the drug is minimal. This can be determined *in vitro* (e.g., hepatocytes (55)) or *in vivo* in real-time (necessary due to short half-life of the isotopes), using the metabolite-to-parent drug concentration ratio in the blood/plasma as a surrogate for the degree of metabolism in the tissue (6). In addition, both PET and γS/SPECT cannot distinguish between the total and unbound drug. However, this disadvantage can be mitigated by correcting the measured tissue drug concentration for binding using the methods described above. For the purposes of verifying the prediction of total tissue drug concentrations from *in vitro* data in conjunction with proteomics and PBPK modeling, this disadvantage is not an issue provided the intracellular binding of the drug in the *in vitro* system is representative of that *in vivo*.

Numerous PET imaging studies have been conducted to quantify tissue distribution and to elucidate the impact of transporter DDIs/polymorphisms on drug tissue exposure. Representative examples summarized in Table 2 focus primarily on the efflux transporters in the blood-brain barrier (BBB), hepatobiliary transporters and quantification of changes in renal exposure relative to systemic.

γ Scintigraphy/SPECT

The imaging agent ^{99m}Tc–mebrofenin (MEB) has been used as a transporter probe to assess liver exposure and DDIs or disease-mediated alterations in hepatic transporter function in humans (56, 57). OATP1B1 and OATP1B3 are responsible for the MEB hepatic uptake, which is rapidly excreted into bile by the canalicular transporter MRP2. MEB is highly extracted by the liver with minimal urinary excretion (~1–2%), moderate protein binding (~90%) and negligible metabolism (See supplemental reading list for more information). MEB liver concentrations were significantly increased in patients with non-alcoholic steatohepatitis (NASH) due to impaired MRP2 function (57). The transporter inhibitor ritonavir at clinically relevant concentrations significantly increased MEB systemic exposure in healthy subjects without affecting overall hepatic exposure or biliary recovery of MEB. *In vitro* studies in human SCH confirmed predictions from the semi-PBPK model that ritonavir inhibited MEB hepatic uptake, but not biliary excretion (56). Advantages of the ^{99m}Tc radiotracer include a suitable half-life (6h), labeling does not require a cyclotron, and gamma cameras are routinely available in health care facilities. However, localization of the ^{99m}Tc label on the substrate may influence the affinity for transporters. For example, OATPs

and MRP2 were primarily responsible for the uptake and efflux, respectively, of ^{99m}Tc-labeled chenodeoxycholic acid and ^{99m}Tc-cholic acid rather than NTCP and BSEP, respectively, due to localization of [^{99m}Tc]-DTPA- on the acidic side chain of the bile acids. Quantitative scintigraphy provides a rich dataset that is ideal for pharmacokinetic modeling but this approach has been underutilized to assess organ/tissue exposure and hepatic transporter DDIs in humans, possibly due to lack of methodological expertise and the limitations cited above.

Contrast-Enhanced Magnetic Resonance Imaging (MRI)

Dynamic gadoxetate-enhanced liver MRI has been used to quantify hepatic transporter function in rodents (58) and humans (59). Gadoxetate is an OATP1B1, OATP1B3 and MRP2 substrate. Gadoxetate is metabolically stable with minimal protein binding (~10%); ~50% of an injected dose is recovered in human urine (See supplemental reading list for more information). Gadoxetate is used routinely in the clinic as a MRI contrast agent, which makes it particularly attractive as a probe to assess hepatic transporter function and DDIs. Physiologically-based (60) and compartmental (61) models have been proposed to describe gadoxetate disposition, but further work is needed to establish an approach to assess hepatic exposure and transporter function in routine clinical workflows.

These imaging studies can provide rich relevant data to verify other methods (e.g., PBPK modeling of transporter disposition) used to predict total tissue drug concentrations. In a recent study (44), *in vivo* rat hepatic concentrations of rosuvastatin (Oatp but not Ntcp substrate in rat, although it is a substrate of human NTCP), determined by PET imaging, were predicted well by combining a proteomics informed bottom-up approach with *in vitro* kinetic data from rat SCH. The proteomic data in tandem with transfected cells expressing each Oatp were used to predict rosuvastatin hepatic uptake clearance, while the rat SCH data were used to predict biliary clearance.

APPLICATION OF PBPK MODELING FOR PREDICTION OF TRANSPORTER-MEDIATED DISPOSITION AND POTENTIAL DISCONNECT BETWEEN SYSTEMIC AND TISSUE DRUG CONCENTRATIONS

Although PBPK models allow simulation of tissue profiles, direct verification of these predictions is typically not possible (Table 3) due to a lack of quantitative tissue drug concentration data (except through imaging, see above). In the case of statins, clinical data on reduction of cholesterol and on muscle toxicity in certain clinical settings have provided indirect verification of the models (3, 62). The time course of statin cholesterol response (>few weeks) is a practical challenge for wider use of this PD endpoint to describe changes in liver exposure as a result of transporter modulation. PBPK modeling explains successfully the observed lack of a significant effect of the *SLCO1B1* c.521T>C polymorphism on the efficacy of both simvastatin acid and rosuvastatin. Opposite trends, i.e., increased efficacy, are seen when either hepatic metabolism (CYP3A4) or biliary excretion (BCRP) are inhibited, consistent with an understanding of the rate-determining processes that affect hepatic AUC of these drugs (2, 3, 63). Recent PET data (Table 2) illustrate the effect of reduced OCT1 activity on metformin hepatic distribution; in this case, the consequences of

reduced hepatic uptake are different from statins, reflecting the importance of predominant non-hepatic (renal) elimination in the case of metformin ($K_{p,uu}$ simulations of such scenarios are shown in Figure S1). In addition, combined PBPK-PD modeling has demonstrated the importance of using simulated liver concentrations to drive the response for rosuvastatin (62). However, confidence in model-simulated tissue concentrations is still low based on limited means to qualify those aspects of the models, and therefore, plasma data are often relied on as a surrogate, with the caveat that variability in plasma PK may not necessarily reflect variability at the site of action.

Extension of PBPK models to predict transporter-mediated PK in specific populations

A number of recently published studies and regulatory submissions have implemented mechanistic liver and kidney models to simulate transporter-mediated disposition/DDIs in organ impairment and/or to extrapolate across ethnic groups/diseased populations (Table 3, Table S3). All these examples highlight limited knowledge or gaps in some physiological/system data such as enzyme or transporter expression/activity and proximal tubule cellularity in diseased kidneys. In order to capture reduced active secretion clearance in renal impairment, models have employed a range of potential mechanisms: reduced proximal tubule cellularity, reduced transporter expression and/or inhibition of renal transporters by uremic solutes (64–66). In some instances reduction of transporter expression proportional to glomerular filtration rate (GFR) was sufficient (e.g., OATP4C1/digoxin), whereas in the case of the OAT1 transporter, more pronounced reduction in activity associated with the inhibitory effect of uremic solutes was required for severe chronic kidney disease (CKD). In all the cases shown, a step-wise model verification against independent clinical data (renal clearance, urinary excretion and/or renal DDI data) was performed. Limited examples of simulated proximal tubule concentrations highlighted that different plausible CKD mechanisms considered in these PBPK models may result in comparable net predicted systemic exposure/renal clearance; however, predicted proximal tubule concentrations may differ depending on the assumptions made (66). The latter may have significant consequences if the model is used subsequently for prospective evaluation of transporter-mediated DDIs/nephrotoxicity risk in patients with severe organ impairment. In addition to physiological changes at the level of the proximal renal tubule, increasing severity of CKD has been reported to have a differential effect on the activity of hepatic enzymes/transporters (e.g., reduced activity of CYP2D6 and OATP1B1, in contrast to variable and marginal effect on CYP3A (67, 68)). These changes need to be considered when model-informed approaches are applied to guide dosing recommendations of nonrenally eliminated drugs in severe CKD patients.

A number of literature and regulatory examples in Table 3 illustrate the use of late stage clinical data to calibrate the missing system or drug-dependent parameters (e.g., transporter-mediated clearance or RAF/REF to account for activity/expression differences between *in vitro* and *in vivo*). Methodological challenges associated with the use of plasma data to inform some of the parameters of the model, structural identifiability concerns and uncertainty associated with parameter estimates have been discussed previously (See supplemental reading list for more information). A general concern is that multiple solutions of the ‘optimized’ parameter may all recapitulate systemic PK exposure reasonably well and

can therefore not be differentiated on the systemic level, yet they will result in differing levels of drug exposure in the tissues. One possible approach to mitigate potential bias is the application of the integrated population PBPK approach, which overcomes reliance on fixed parameters by using a Bayesian framework. This method generates a statistical distribution of the output parameters, rather than just a single estimate. However, rich clinical data are required to update the priors in this 'reverse translation' exercise and hence would not be applicable for early stages of model development. Further, while this addresses the data limitations in the most robust fashion, it still may not result in improved precision in predicting changes in tissue concentrations.

Key points from transporter PBPK regulatory cases

Regulatory submissions of PBPK modeling have included simulations of transporter-mediated DDIs as well as simulations of tissue concentrations (e.g., liver) in the context of evaluating the need for dosage adjustment due to patient factors, as exemplified by simeprevir and obeticholic acid (OCA).

The simeprevir PBPK model incorporated saturable CYP3A4 and OATP1B kinetics, and was used to investigate DDI risk for a number of untested clinical interactions ((69), Table 3). Higher simeprevir plasma exposure was predicted when moderate/strong CYP3A inhibitors were co-administered with multiple-doses of simeprevir compared with a single-dose due to the saturation of CYP3A4/OATP1B. Concomitant administration of moderate/strong CYP3A inhibitors are not recommended per simeprevir US labeling. Simeprevir PBPK modeling was also used to evaluate changes in liver concentrations (70) as the target organ (PBPK-PD details shown in Case Study 3). Simulations of 100 mg daily administration in Chinese and Japanese patients and 150 mg daily in Caucasian patients resulted in comparable predicted liver exposure in the Chinese and Japanese population. Although no dose adjustment was initially recommended based on ethnicity, 150 mg QD is the approved regimen in the FDA label and 100 mg QD is the recommended dose in the Pharmaceuticals and Medical Devices Agency (PMDA) label. The FDA also issued a post-marketing requirement for simeprevir to evaluate safety signals in patients with East Asian ancestry.

In the case of OCA, PBPK modelling was used to predict steady-state plasma and liver exposures in subjects with different degrees of hepatic impairment. Considering significantly higher predicted OCA plasma exposure and liver-related adverse reactions, a less frequent starting dosage regimen was recommended in patients with moderate or severe hepatic impairment (from 5 mg daily to 5 mg weekly). Unfortunately, since approval, severe liver injury and deaths have been reported in patients with moderate/severe hepatic impairment when OCA was dosed more frequently than recommended. Consequently, a 'Dear Healthcare Provider' letter by the applicant and a Drug Safety Communication by the FDA were issued to warn about OCA liver toxicity and emphasize adherence to recommended dosing regimens in patients with moderate or severe hepatic impairment.

In the cases highlighted above, PBPK modelling enabled assessment of transporter-metabolism interplay and the impact of physiological differences associated with organ disease or ethnicity on plasma/tissue exposure. This integrative platform was used to bridge

the differences between changes in systemic and tissue concentrations (where relevant) to support important regulatory decisions for the ultimate goal of optimizing patient benefit. As illustrated in case examples below, the structure and complexity of the selected model/modeling approach depend both on the key questions and the availability of the physiological, *in vitro, in vivo* (plasma or tissue) and/or PD data necessary to describe and verify multiple processes/parameters in the model.

Case Study 1—Consideration of intracellular drug concentrations is critical when estimating a starting dose for the first clinical study with a novel therapeutic that is actively transported to an intracellular site of action, as illustrated in this example for a novel Hepatitis B Virus (HBV) inhibitor. The molecule exhibited low passive membrane permeability *in vitro* and was a substrate of OATP1B1 and OATP1B3 (transfected CHO cells) and BCRP (transfected MDCKII cells), but was not a P-gp substrate (71) (Table S4). *In vitro* inhibition of viral DNA production was measured in hepatoma cell lines HepG2.2.15 and HepaRG, but translation of *in vitro* potency to *in vivo* was challenging as these systems are deficient in baseline drug transport/metabolic activities, so the $K_{p,uu}$ is not expected to mimic the situation in human hepatocytes. Additionally, PKPD studies in mice were performed to characterize HBV DNA inhibition *in vivo*. Translation of efficacy from these animal data faces the challenge that the specific transporters involved in hepatic disposition in rodents were not known. However, primary plated rat and human hepatocytes both showed active contributions amounting to ~70% of the total uptake, supportive of a similar relationship between hepatic intracellular and plasma concentrations in rodents and humans. PKPD modeling with mouse data estimated a trough concentration above which plasma concentrations should lie throughout the dosing interval and this was used as the target for estimation of an efficacious dose in humans.

For the prediction of human pharmacokinetics, a published strategy was followed (72) whereby PBPK simulations were first verified in mouse, rat, dog and monkey before prediction of human PK. Simulations in preclinical species were compared to measured plasma and tissue concentrations obtained after intravenous and oral administration. The volume of distribution (Vss) predicted from physicochemical and drug binding properties, and assuming passive diffusion across membranes (73), underestimated the measured volume in all the preclinical species. After adjusting for the measured liver K_p in mice and rats that were ~100-fold higher than predicted, the predicted and observed Vss were in better agreement in these species. Therefore, the measured human hepatocyte K_p of ~80 was incorporated in the liver compartment of the human PBPK model. This approach predicted a human Vss of 1 L/kg.

In vitro measurements in liver microsomes showed low intrinsic clearance (CL_{int}) across species, which could not be reconciled with the moderate to high *in vivo* clearance in the animal species. Although higher CL_{int} values were measured in hepatocyte suspensions, the CL_{int} was below a reliable quantitative level for this assay (<3μL/min/million cells). Therefore, to obtain a more precise estimate, measurements were repeated in a long-term human hepatocyte co-culture system that may provide an improved representation of combined contributions of uptake, metabolism and biliary excretion to total hepatic clearance (71). CL_{int} obtained was scaled using the physiologically-based approach resulting

in a human plasma clearance of 7.4 mL/min/kg which was higher than the value predicted with the suspension data. A good agreement between simulations and clinical PK data at low doses was observed (Figure 2). However, for doses of 300 mg and above, the observed plasma concentrations increased greater than proportionally with the dose, leading to average fold-errors of 4.4 for C_{max} and 2.2 for AUC. An error of >2-fold in the PBPK predicted PK parameters is beyond typical values for permeable molecules with clearance mainly determined by metabolism, which exemplifies the current lack of confidence in PBPK predictions for transported drugs (74). Unfortunately, intravenous PK data were not available, which limited definitive conclusions on the reasons for the poorly predicted PK of this molecule at higher doses. The over-proportional increases in oral exposure are likely due to saturation of clearance processes. However, such saturation was not anticipated based on the available *in vitro* data. Once clinical data were available, top-down fitting of plasma concentrations across the full dose range estimated that an uptake transporter K_m of ~0.2 μM would recover the observed nonlinearity.

This case study illustrates an example where infection of the co-culture model with patient-derived HBV has been demonstrated (71). This opens the possibility to use this cellular system to develop more relevant PKPD models that account for the relationship between human plasma and intracellular concentrations. In addition, the case study highlights the potential translational application of more holistic *in vitro* co-culture systems for evaluation of complex transporter-metabolism interplay. However, there are still gaps in understanding, as shown in the disconnect between *in vitro* and *in vivo* nonlinearity reported here, and more detailed characterization of these models is necessary to appreciate their full potential.

Case Study 2—This example illustrates the use of PBPK modeling to characterize unanticipated nonlinear human PK that may arise through saturation of transporter-mediated hepatic uptake, and to explain differences in PK in different populations for letermovir. Letermovir is a novel drug inhibiting the human cytomegalovirus virus (CMV) terminase complex recently approved for prophylaxis of clinically significant CMV infection (properties in Table S4). Letermovir is a substrate of OATP1B1, and -1B3 (transfected CHO cells) and is metabolized by CYP3A4, UGT1A1 and UGT1A3 (data from recombinant enzymes). As summarized in the disposition characteristics of letermovir (Figure 3A), the model assumed that OATP1B1 is responsible for its saturable active uptake into the liver; the CL_{int} via glucuronidation was assigned to UGT1A1. Recovery of intact parent in feces is primarily due to biliary excretion of absorbed drug (estimated bioavailability of ~90%).

The workflow of letermovir PBPK model development and the model qualification plan is summarized in Figure 3B. The PBPK model was able to capture the nonlinear PK of letermovir in Caucasian healthy subjects after receiving single doses of letermovir across the dose range of 120 to 720 mg IV and 120 to 480 mg PO (Figure 3C and 3D). The mechanism of nonlinear PK of letermovir was best described by saturation of OATP1B-mediated hepatic uptake. The exposure of letermovir in Japanese healthy subjects is ~2-fold higher than in Caucasians. A population PK analysis identified weight as the primary contributor to this higher exposure (unpublished results). Accounting for known demographic and physiological differences (body weight and liver mass) in the PBPK model explained some of the differences in PK exposure (Table S5). It was hypothesized that reported differences

in abundance and/or activities of hepatic OATP1B contribute to the higher systemic exposure observed in Japanese due to reduced hepatic uptake (75). To explore this hypothesis by simulation, the abundance of OATP1B in Japanese subjects was assigned a value of 0.58 (75). Simulations were in good agreement with the observed data, and support the hypothesis that the higher exposure in Japanese as compared to Caucasian healthy subjects may be rationalized by contributions both from known physiological differences between these two populations and differences in hepatic uptake due to transporter OATP1B abundance and/or activities.

In addition, the PBPK model was used to evaluate the hypothesis that reduced absorption, likely caused by mucositis, could be the cause for decreased exposure observed in hematopoietic stem cell transplant (HSCT) recipients after oral administration of 480 mg letermovir. To evaluate this by simulation, the Caucasian healthy subject PBPK model was modified to account for reduced ka and fraction absorbed using a sensitivity analysis approach. The simulations showed that the PK in HSCT recipients after oral administration of 480 mg letermovir was best described by a reduction in the fraction absorbed, consistent with previous reports of reduced exposure for orally administered drugs in HSCT recipients (76). This case study illustrates challenges encountered in PBPK modeling and simulation of transporter-mediated disposition and approaches used to rationalize the nonlinear PK and observed differences in PK between populations to guide the product development team and subsequent regulatory submission.

Case Study 3—Simeprevir is a hepatitis C virus (HCV) NS3/4A protease inhibitor (PI), indicated for the treatment of HCV genotype 1 and genotype 4 infections (69). Simeprevir is characterized by low solubility and low permeability (properties detailed in (69)). Simeprevir is actively taken up into hepatocytes by OATP1B1/OATP1B3, followed by metabolism via CYP3A4, and biliary elimination of parent drug and metabolites. PBPK modeling was conducted to simulate simeprevir exposure in the liver in different patient populations and in DDI studies (Table 3). To evaluate whether the PBPK simulated liver exposures could be linked to simeprevir PD, an effort was initiated to compare the simulated liver exposures with the estimated liver exposures based on the observed PD effect of simeprevir on HCV RNA. Adapting the modeling approaches developed by Ke *et al.* (77), simeprevir PK, PD and viral dynamics (viral load (VL) data) were used to estimate the ratio between simeprevir plasma (Cplasma) and liver (Cliver) concentrations *in vivo* (Table S6). VL data from clinical studies with simeprevir monotherapy (5 or 7 days) in treatment-experienced or treatment-naïve patients were used after 3 days of treatment to ensure that VL had reached quasi-equilibrium, i.e., the reduction in VL was set by the clearance rate of infected cells. The baseline PD serum shifted EC_{50} values for every subject in the clinical simeprevir monotherapy studies were derived *in vitro* in chimeric replicon cells using the HCV virus from every individual subject, which enabled generation of subject-specific EC_{50} values for simeprevir. The outcome of this exercise shows that the PBPK simulated liver-to-plasma ratios of simeprevir are in very good agreement with the values based on the top-down viral kinetic, PK and PD mathematical modeling. One of the drivers of the nonlinear simeprevir plasma PK in the PBPK simulations was the saturation of active hepatic uptake at simeprevir doses above 100 mg daily, which was reflected in lower simeprevir liver K_p

values at doses above 100 mg daily relative to lower doses. Intriguingly, the top-down approach also showed a trend towards a 2-fold lower liver K_p at the 200 mg daily dose versus the 25 and 75 mg doses. This case study illustrates the indirect evaluation of the PBPK-simulated tissue exposure using the PD data and highlights the importance of using local tissue concentrations to drive the PD effect.

FUTURE DIRECTIONS

This white paper provides current best practices for the estimation of tissue and intra/subcellular drug concentrations and their advantages/limitations in clinical translation. These approaches have been integrated into a quantitative framework in the context of drug development (Figure 4) to illustrate how *in vitro*, preclinical, imaging, early and late clinical data can be utilized to examine plasma and tissue exposure in case of transporter-mediated issues. The choice of methods and data considered depend on compound properties and stages of drug development; each institution may need to establish consistent internal approaches for selection of *in vitro* and preclinical systems and parameter estimates.

Advances in the following areas may facilitate progress in predicting and verifying unbound tissue drug concentrations. First, optimization of *in vitro* incubation conditions and increased availability of preclinical *in vivo* $K_{p,uu}$ data (obtained under steady-state conditions and modeled appropriately) are required to improve IVIVC of *in vitro* $K_{p,uu}$ data and inform subsequent human predictions (Figure 4). Second, integrated approaches illustrated here (e.g., combination of proteomics informed bottom-up PBPK modeling and imaging data) are needed. In this regard, additional imaging studies with model transporter substrates will facilitate this process. Further studies to determine whether all hepatic clearance pathways (and therefore hepatic drug concentrations) can be simultaneously predicted from certain cell systems (e.g., human SCH) or integrated from a range of systems (e.g., knockout/transfected cell lines combined with data from human liver microsomal/S9) are required. Such studies have been reported for the liver (44), brain (e.g. (78)) and kidneys (50) and need to be extended to the intestine. With regard to estimation of subcellular concentrations, methods are needed to directly measure drug concentrations in lysosomes and mitochondria to allow verification of current *in silico* predictions. Improved understanding of uncertainty associated with some of the cellular parameters such as acidic phospholipid content, composition of organelle membranes relative to the plasma membrane, and the impact of pathophysiological conditions on these parameters, is envisaged to improve performance of *in silico* cellular models. Fatty acid binding proteins have recently emerged as important cytosolic binding proteins that chaperone very lipophilic molecules, such as endocannabinoids and cannabinoids, to intracellular targets for metabolism in the brain and liver (79). Continued research is needed to elucidate the impact of alterations in levels and/or binding affinity of chaperone fatty-acid binding proteins on unbound intracellular drug concentrations and subsequently, efficacy and toxicity. Finally, utility of microphysiological systems (80) for quantitative translation of transporter data, understanding of tissue concentrations/complex transporter-mediated DDIs and/or their potential for PKPD characterization remains to be established.

Modeling examples summarized from the literature, regulatory submissions or drug development case studies highlight the importance of informative clinical data for model verification and/or parameter optimization. For example, urinary excretion data is necessary for the optimization of REF/kinetic parameters for transporters expressed on the apical membrane of renal proximal tubule cells (e.g., MATEs) (51), whereas plasma data are sufficient for optimization of basolateral transporters (e.g., OAT3, (48)). Some examples in this white paper illustrate scenarios where efficacy and safety of a drug were linked to model-predicted tissue concentrations rather than surrogate plasma concentrations. It is envisaged that increased availability of quantitative PET/MRI tissue data will refine/'re-qualify' existing PBPK models for clinical transporter probes to improve translation of transporter-mediated tissue distribution and increase confidence in the design of prospective DDI studies (in combination with corresponding perpetrator PBPK model(s) and monitoring of endogenous transporter biomarkers, Figure 4). There is an increasing interest in using PBPK modeling to support dose optimization in organ impairment and understand the impact of disease on tissue exposure and transporter-mediated DDIs (often in conjunction with metabolic enzymes). Although existing mechanistic kidney models account for regional differences in blood and tubular fluid flows, implementation of heterogeneity in transporter and enzyme expression and regional scalars is still evolving as the data become available. Current mechanistic kidney and liver models have not yet implemented the impact of pH on transporter activity, or accounted for potential transporter trafficking. Transporter bidirectionality, electrochemical gradient driven transport (as proposed for OCT2, (51)), and basolateral efflux may all affect our understanding of major transporters driving hepatic/renal clearance and corresponding DDIs. Further work and increased confidence is required for the application of pediatric PBPK models for drugs with transporter-mediated disposition, especially considering increased interest in model-informed dose recommendations for this patient population (81, 82). Refinement or bridging the knowledge gaps in systems parameters is required in the areas of transporter expression and ontogeny (53, 83, 84). Similarly, a number of studies suggest that differences in exposure to drugs that are OATP1B1 substrates between Japanese and Caucasians may not be solely attributed to differences in transporter activity/expression or genotype (75, 85, 86), highlighting challenges in extrapolating transporter-mediated PK across ethnic groups. All of the above, in conjunction with the potential interplay of transporters with metabolites (especially conjugates), both in the liver (enterohepatic circulation) and the kidney (87, 88), highlight areas for further work of relevance for predicting tissue/subcellular drug concentrations, clearance of drugs and complex DDIs.

Supplementary Material

Refer to Web version on PubMed Central for supplementary material.

Acknowledgments

Funding: This work was supported, in part, by funding from the National Institutes of Health through award numbers R01 GM041935 (KLRB), R35 GM122576 (KLRB), 1R01GM104178 (SN), and 1R01GM114369 (SN) from the National Institute of General Medical Sciences, and DA P01DA032507 (JDU).

The authors acknowledge Haoxun Wang (Rutgers, The State University of New Jersey) for help with Tables 1 and 2, Eva Sherbetjian (University of Manchester) for help with Table 2 and Gabriela Patilea-Vrana (University of

Washington) for help with Figure 1 and Figure S1. The authors would like to acknowledge members of the ITC for their valuable comments on the manuscript.

Abbreviations

BBB
blood-brain barrier

B/P
blood to plasma ratio

CHO cells
Chinese hamster ovary cells

CKD
chronic kidney disease

C_{liver}
liver concentration

CL_{int}
intrinsic clearance

$CL^{s}_{in,act}$
sinusoidal active influx clearance

$CL^{s}_{ef,act}$
sinusoidal active efflux clearance

CL_{dif}
passive diffusion

CL_{bile}
canalicular efflux (biliary) clearance

CL_{met}
metabolic clearance

CMV
cytomegalovirus

C_{plasma}
plasma concentration

DDI
drug-drug interactions

ECM
Extended Clearance Model

Fa
fraction absorbed

$f_{u,brain}$
fraction unbound in brain

$f_{u,cell}$
fraction unbound in cell

$f_{u,liver}$
fraction unbound in liver

$f_{u,medium}$
fraction unbound in medium

$f_{u,p}$
fraction unbound in plasma

Gadoxetate, Gd-EOB-DTPA
gadolinium-ethoxybenzyl-diethylenetriame-pentaacetic acid

GFR
glomerular filtration rate

HCV
hepatitis C virus

HEK293 cells
human embryonic kidney 293 cells

HIDA
hepatobiliary imino diacetic acid

HSCT
hematopoietic stem cell transplant

HV
healthy volunteers

ka
oral absorption rates

IVIVC
in vitro-in vivo correlation

IVIVE
In vitro-in vivo extrapolation

K_p
total cell to medium concentration ratio or measured tissue partition coefficients

$K_{p,u}$
total cell-to-unbound medium concentration ratio

$K_{p,uu}$
steady-state unbound tissue-to-blood partition coefficient

LogP
log octanol:water partition coefficient

MEB
^{99m}Tc–mebrofenin

MRI
magnetic resonance imaging

MSI
mass spectrometry imaging

MW
Molecular Weight

NASH
non-alcoholic steatohepatitis

NH_4Cl
ammonium chloride

OCA
obeticholic acid

P_{app}
apparent permeability

PBPK
Physiologically-based pharmacokinetic

PD
pharmacodynamics

PET
positron emission tomography

PI
protease inhibitor

PK
pharmacokinetic

pKa
log acid dissociation constant

PMDA
Pharmaceuticals and Medical Devices Agency

RAF
relative activity factor

REF
relative expression factor

SCH
sandwich-cultured hepatocytes

SPECT
single-photon emission computed tomography

VL
viral load

Vss
apparent volume of distribution.

References

1. Galetin A, Zhao P, Huang SM. Physiologically Based Pharmacokinetic Modeling of Drug Transporters to Facilitate Individualized Dose Prediction. J Pharm Sci. 2017; 106:2204–8. [PubMed: 28390843]
2. Chu X, et al. Intracellular drug concentrations and transporters: measurement, modeling, and implications for the liver. Clin Pharmacol Ther. 2013; 94:126–41. [PubMed: 23588320]
3. Tsamandouras N, et al. Development and Application of a Mechanistic Pharmacokinetic Model for Simvastatin and its Active Metabolite Simvastatin Acid Using an Integrated Population PBPK Approach. Pharm Res. 2015; 32:1864–83. [PubMed: 25446771]
4. Patilea-Vrana G, Unadkat JD. Transport vs. Metabolism: What Determines the Pharmacokinetics and Pharmacodynamics of Drugs? Insights From the Extended Clearance Model. Clin Pharmacol Ther. 2016; 100:413–8. [PubMed: 27448198]
5. Varma MV, et al. Extended Clearance Classification System (ECCS) Informed Approach for Evaluating Investigational Drugs as Substrates of Drug Transporters. Clin Pharmacol Ther. 2016
6. Sasongko L, et al. Imaging P-glycoprotein transport activity at the human blood-brain barrier with positron emission tomography. Clin Pharmacol Ther. 2005; 77:503–14. [PubMed: 15961982]
7. Hibma JE, et al. The Effect of Famotidine, a MATE1-Selective Inhibitor, on the Pharmacokinetics and Pharmacodynamics of Metformin. Clin Pharmacokinet. 2016; 55:711–21. [PubMed: 26597253]
8. Lai Y, Tse CM, Unadkat JD. Mitochondrial expression of the human equilibrative nucleoside transporter 1 (hENT1) results in enhanced mitochondrial toxicity of antiviral drugs. J Biol Chem. 2004; 279:4490–7. [PubMed: 14607828]
9. Yoshida K, Maeda K, Sugiyama Y. Hepatic and intestinal drug transporters: prediction of pharmacokinetic effects caused by drug-drug interactions and genetic polymorphisms. Annu Rev Pharmacol Toxicol. 2013; 53:581–612. [PubMed: 23140240]
10. Zamek-Gliszczynski MJ, et al. ITC recommendations for transporter kinetic parameter estimation and translational modeling of transport-mediated PK and DDIs in humans. Clin Pharmacol Ther. 2013; 94:64–79. [PubMed: 23588311]
11. Rostami-Hodjegan A. Reverse Translation in PBPK and QSP: Going Backwards in Order to Go Forward With Confidence. Clin Pharmacol Ther. 2018; 103:224–32. [PubMed: 29023678]

12. Mateus A, Matsson P, Artursson P. Rapid measurement of intracellular unbound drug concentrations. Mol Pharm. 2013; 10:2467–78. [PubMed: 23631740]
13. Pfeifer ND, Harris KB, Yan GZ, Brouwer KL. Determination of intracellular unbound concentrations and subcellular localization of drugs in rat sandwich-cultured hepatocytes compared with liver tissue. Drug Metab Dispos. 2013; 41:1949–56. [PubMed: 23990525]
14. Riccardi K, et al. Novel Method to Predict In Vivo Liver-to-Plasma Kpuu for OATP Substrates Using Suspension Hepatocytes. Drug Metab Dispos. 2017; 45:576–80. [PubMed: 28258068]
15. Riede J, Camenisch G, Huwyler J, Poller B. Current In Vitro Methods to Determine Hepatic Kpuu: A Comparison of Their Usefulness and Limitations. J Pharm Sci. 2017; 106:2805–14. [PubMed: 28385545]
16. Shitara Y, Maeda K, Ikejiri K, Yoshida K, Horie T, Sugiyama Y. Clinical significance of organic anion transporting polypeptides (OATPs) in drug disposition: their roles in hepatic clearance and intestinal absorption. Biopharm Drug Dispos. 2013; 34:45–78. [PubMed: 23115084]
17. Yoshikado T, et al. Comparison of Methods for Estimating Unbound Intracellular-to-Medium Concentration Ratios in Rat and Human Hepatocytes Using Statins. Drug Metab Dispos. 2017; 45:779–89. [PubMed: 28468836]
18. Yabe Y, Galetin A, Houston JB. Kinetic characterization of rat hepatic uptake of 16 actively transported drugs. Drug Metab Dispos. 2011; 39:1808–14. [PubMed: 21730030]
19. Riccardi KA, et al. Comparison of Species and Cell-Type Differences in Fraction Unbound of Liver Tissues, Hepatocytes and Cell-Lines. Drug Metab Dispos. 2018
20. Miyauchi S, et al. The Phenomenon of Albumin-Mediated Hepatic Uptake of Organic Anion Transport Polypeptide Substrates: Prediction of the In Vivo Uptake Clearance from the In Vitro Uptake by Isolated Hepatocytes Using a Facilitated-Dissociation Model. Drug Metab Dispos. 2018; 46:259–67. [PubMed: 29298773]
21. Kulkarni P, Korzekwa K, Nagar S. Intracellular Unbound Atorvastatin Concentrations in the Presence of Metabolism and Transport. J Pharmacol Exp Ther. 2016; 359:26–36. [PubMed: 27451408]
22. Menochet K, Kenworthy KE, Houston JB, Galetin A. Use of mechanistic modeling to assess interindividual variability and interspecies differences in active uptake in human and rat hepatocytes. Drug Metab Dispos. 2012; 40:1744–56. [PubMed: 22665271]
23. Ufuk A, Somers G, Houston JB, Galetin A. In Vitro Assessment of Uptake and Lysosomal Sequestration of Respiratory Drugs in Alveolar Macrophage Cell Line NR8383. Pharm Res. 2015; 32:3937–51. [PubMed: 26224396]
24. Kaufmann AM, Krise JP. Lysosomal sequestration of amine-containing drugs: analysis and therapeutic implications. J Pharm Sci. 2007; 96:729–46. [PubMed: 17117426]
25. Francis L, Harrell A, Hallifax D, Galetin A. Novel methodology for the isolation of lysosomes and measurement of intralysosomal drug accumulation. 14th European ISSX Meeting; Cologne Germany. 2017.
26. Trapp S, Rosania GR, Horobin RW, Kornhuber J. Quantitative modeling of selective lysosomal targeting for drug design. Eur Biophys J. 2008; 37:1317–28. [PubMed: 18504571]
27. Ufuk A, et al. In Vitro and in Silico Tools To Assess Extent of Cellular Uptake and Lysosomal Sequestration of Respiratory Drugs in Human Alveolar Macrophages. Mol Pharm. 2017; 14:1033–46. [PubMed: 28252969]
28. Assmus F, Houston JB, Galetin A. Incorporation of lysosomal sequestration in the mechanistic model for prediction of tissue distribution of basic drugs. Eur J Pharm Sci. 2017; 109:419–30. [PubMed: 28823852]
29. Ghosh A, et al. Toward a unified model of passive drug permeation II: the physiochemical determinants of unbound tissue distribution with applications to the design of hepatoselective glucokinase activators. Drug Metab Dispos. 2014; 42:1599–610. [PubMed: 25024402]
30. Chien HC, et al. Rapid Method To Determine Intracellular Drug Concentrations in Cellular Uptake Assays: Application to Metformin in Organic Cation Transporter 1-Transfected Human Embryonic Kidney 293 Cells. Drug Metab Dispos. 2016; 44:356–64. [PubMed: 26700958]
31. Gordon LJ, et al. Direct Measurement of Intracellular Compound Concentration by RapidFire Mass Spectrometry Offers Insights into Cell Permeability. J Biomol Screen. 2017; 21:156–64.

32. Mateus A, Treyer A, Wegler C, Karlgren M, Matsson P, Artursson P. Intracellular drug bioavailability: a new predictor of system dependent drug disposition. Sci Rep. 2017; 7:43047. [PubMed: 28225057]
33. Cantrill C, Houston JB. Understanding the Interplay Between Uptake and Efflux Transporters Within In Vitro Systems in Defining Hepatocellular Drug Concentrations. J Pharm Sci. 2017; 106:2815–25. [PubMed: 28478131]
34. Guo C, Yang K, Liao M, Xia CQ, Brouwer KR, Brouwer KLR. Prediction of Hepatic Efflux Transporter-Mediated Drug Interactions: When Is it Optimal to Measure Intracellular Unbound Fraction of Inhibitors? J Pharm Sci. 2017; 106:2401–6. [PubMed: 28465154]
35. Mateus A, Matsson P, Artursson P. A high-throughput cell-based method to predict the unbound drug fraction in the brain. J Med Chem. 2014; 57:3005–10. [PubMed: 24601604]
36. Riede J, Poller B, Huwyler J, Camenisch G. Assessing the Risk of Drug-Induced Cholestasis Using Unbound Intrahepatic Concentrations. Drug Metab Dispos. 2017; 45:523–31. [PubMed: 28254950]
37. Dawson S, Stahl S, Paul N, Barber J, Kenna JG. In vitro inhibition of the bile salt export pump correlates with risk of cholestatic drug-induced liver injury in humans. Drug Metab Dispos. 2012; 40:130–8. [PubMed: 21965623]
38. Durmus S, Lozano-Mena G, van Esch A, Wagenaar E, van Tellingen O, Schinkel AH. Preclinical Mouse Models To Study Human OATP1B1- and OATP1B3-Mediated Drug-Drug Interactions in Vivo. Mol Pharm. 2015; 12:4259–69. [PubMed: 26474710]
39. Higgins JW, et al. Utility of Oatp1a/1b-knockout and OATP1B1/3-humanized mice in the study of OATP-mediated pharmacokinetics and tissue distribution: case studies with pravastatin, atorvastatin, simvastatin, and carboxydichlorofluorescein. Drug Metab Dispos. 2014; 42:182–92. [PubMed: 24194513]
40. Chu X, Bleasby K, Evers R. Species differences in drug transporters and implications for translating preclinical findings to humans. Expert Opin Drug Metab Toxicol. 2013; 9:237–52. [PubMed: 23256482]
41. Izumi S, et al. Comparison of the Predictability of Human Hepatic Clearance for Organic Anion Transporting Polypeptide Substrate Drugs Between Different In Vitro-In Vivo Extrapolation Approaches. J Pharm Sci. 2017; 106:2678–87. [PubMed: 28238896]
42. Badee J, Achour B, Rostami-Hodjegan A, Galetin A. Meta-analysis of expression of hepatic organic anion-transporting polypeptide (OATP) transporters in cellular systems relative to human liver tissue. Drug Metab Dispos. 2015; 43:424–32. [PubMed: 25564656]
43. Burt HJ, Riedmaier AE, Harwood MD, Crewe HK, Gill KL, Neuhoff S. Abundance of Hepatic Transporters in Caucasians: A Meta-Analysis. Drug Metab Dispos. 2016; 44:1550–61. [PubMed: 27493152]
44. Ishida K, Ullah M, Toth B, Juhasz V, Unadkat JD. Successful prediction of in vivo hepatobiliary clearances and hepatic concentrations of rosuvastatin using sandwich-cultured rat hepatocytes, transporter-expressing cell lines, and quantitative proteomics. Drug Metab Dispos. 2017
45. Vildhede A, Wisniewski JR, Noren A, Karlgren M, Artursson P. Comparative Proteomic Analysis of Human Liver Tissue and Isolated Hepatocytes with a Focus on Proteins Determining Drug Exposure. J Proteome Res. 2015; 14:3305–14. [PubMed: 26167961]
46. Chen B, et al. Strategies of Drug Transporter Quantitation by LC-MS: Importance of Peptide Selection and Digestion Efficiency. Aaps J. 2017; 19:1469–78. [PubMed: 28589509]
47. Wegler C, et al. Variability in Mass Spectrometry-based Quantification of Clinically Relevant Drug Transporters and Drug Metabolizing Enzymes. Mol Pharm. 2017; 14:3142–51. [PubMed: 28767254]
48. Posada MM, et al. Prediction of Transporter-Mediated Drug-Drug Interactions for Baricitinib. Clin Transl Sci. 2017; 10:509–19. [PubMed: 28749581]
49. Posada MM, et al. Prediction of renal transporter mediated drug-drug interactions for pemetrexed using physiologically based pharmacokinetic modeling. Drug Metab Dispos. 2015; 43:325–34. [PubMed: 25504564]
50. Mathialagan S, Piotrowski MA, Tess DA, Feng B, Litchfield J, Varma MV. Quantitative Prediction of Human Renal Clearance and Drug-Drug Interactions of Organic Anion Transporter Substrates

Using In Vitro Transport Data: A Relative Activity Factor Approach. Drug Metab Dispos. 2017; 45:409–17. [PubMed: 28179375]

51. Burt HJ, et al. Metformin and cimetidine: Physiologically based pharmacokinetic modelling to investigate transporter mediated drug-drug interactions. Eur J Pharm Sci. 2016; 88:70–82. [PubMed: 27019345]
52. Wang L, et al. Transporter Expression in Liver Tissue from Subjects with Alcoholic or Hepatitis C Cirrhosis Quantified by Targeted Quantitative Proteomics. Drug Metab Dispos. 2016; 44:1752–8. [PubMed: 27543206]
53. Prasad B, et al. Ontogeny of Hepatic Drug Transporters as Quantified by LC-MS/MS Proteomics. Clin Pharmacol Ther. 2016; 100:362–70. [PubMed: 27301780]
54. Langer O. Use of PET Imaging to Evaluate Transporter-Mediated Drug-Drug Interactions. J Clin Pharmacol. 2016; 56(Suppl 7):S143–56. [PubMed: 27385172]
55. Shingaki T, et al. Evaluation of Oatp and Mrp2 activities in hepatobiliary excretion using newly developed positron emission tomography tracer [11C]dehydropravastatin in rats. J Pharmacol Exp Ther. 2013; 347:193–202. [PubMed: 23926287]
56. Pfeifer ND, et al. Effect of Ritonavir on (99m)Technetium-Mebrofenin Disposition in Humans: A Semi-PBPK Modeling and In Vitro Approach to Predict Transporter-Mediated DDIs. CPT Pharmacometrics Syst Pharmacol. 2013; 2:e20. [PubMed: 23887590]
57. Ali I, et al. Transporter-mediated Alterations in Patients with NASH Increase Systemic and Hepatic Exposure to an OATP and MRP2 Substrate. Clin Pharmacol Ther. 2017
58. Ulloa JL, et al. Assessment of gadoxetate DCE-MRI as a biomarker of hepatobiliary transporter inhibition. NMR Biomed. 2013; 26:1258–70. [PubMed: 23564602]
59. Nassif A, et al. Visualization of hepatic uptake transporter function in healthy subjects by using gadoxetic acid-enhanced MR imaging. Radiology. 2012; 264:741–50. [PubMed: 22771883]
60. Forsgren MF, Dahlqvist Leinhard O, Dahlstrom N, Cedersund G, Lundberg P. Physiologically realistic and validated mathematical liver model reveals [corrected] hepatobiliary transfer rates for Gd-EOB-DTPA using human DCE-MRI data. PLoS One. 2014; 9:e95700. [PubMed: 24748411]
61. Giraudeau C, et al. Gadoxetate-enhanced MR imaging and compartmental modelling to assess hepatocyte bidirectional transport function in rats with advanced liver fibrosis. Eur Radiol. 2016; 27:1804–11. [PubMed: 27553933]
62. Rose RH, Neuhoff S, Abduljalil K, Chetty M, Rostami-Hodjegan A, Jamei M. Application of a Physiologically Based Pharmacokinetic Model to Predict OATP1B1-Related Variability in Pharmacodynamics of Rosuvastatin. CPT Pharmacometrics Syst Pharmacol. 2014; 3:e124. [PubMed: 25006781]
63. Lee CA, et al. Breast cancer resistance protein (ABCG2) in clinical pharmacokinetics and drug interactions: practical recommendations for clinical victim and perpetrator drug-drug interaction study design. Drug Metab Dispos. 2015; 43:490–509. [PubMed: 25587128]
64. Hsu V, et al. Towards quantitation of the effects of renal impairment and probenecid inhibition on kidney uptake and efflux transporters, using physiologically based pharmacokinetic modelling and simulations. Clin Pharmacokinet. 2014; 53:283–93. [PubMed: 24214317]
65. Hsueh CH, Hsu V, Zhao P, Zhang L, Giacomini KM, Huang SM. PBPK Modeling of the Effect of Reduced Kidney Function on the Pharmacokinetics of Drugs Excreted Renally by Organic Anion Transporters. Clinical pharmacology and therapeutics. 2018; 103:485–92. [PubMed: 28738449]
66. Scotcher D, Jones CR, Galetin A, Rostami-Hodjegan A. Delineating the Role of Various Factors in Renal Disposition of Digoxin through Application of Physiologically Based Kidney Model to Renal Impairment Populations. J Pharmacol Exp Ther. 2017; 360:484–95. [PubMed: 28057840]
67. Tan ML, et al. Effect of Chronic Kidney Disease on Nonrenal Elimination Pathways: A Systematic Assessment of CYP1A2, CYP2C8, CYP2C9, CYP2C19, and OATP. Clin Pharmacol Ther. 2018; 103:854–67. [PubMed: 28990182]
68. Yoshida K, et al. Systematic and quantitative assessment of the effect of chronic kidney disease on CYP2D6 and CYP3A4/5. Clin Pharmacol Ther. 2016; 100:75–87. [PubMed: 26800425]
69. Snoeys J, Beumont M, Monshouwer M, Ouwerkerk-Mahadevan S. Mechanistic understanding of the nonlinear pharmacokinetics and intersubject variability of simeprevir: A PBPK-guided drug development approach. Clin Pharmacol Ther. 2016; 99:224–34. [PubMed: 26259716]

70. Snoeys J, Beumont M, Monshouwer M, Ouwerkerk-Mahadevan S. Elucidating the Plasma and Liver Pharmacokinetics of Simeprevir in Special Populations Using Physiologically Based Pharmacokinetic Modelling. Clin Pharmacokinet. 2017; 56:781–92. [PubMed: 27896690]
71. Kratochwil NA, et al. Simultaneous Assessment of Clearance, Metabolism, Induction, and Drug-Drug Interaction Potential Using a Long-Term In Vitro Liver Model for a Novel Hepatitis B Virus Inhibitor. J Pharmacol Exp Ther. 2018; 365:237–48. [PubMed: 29453199]
72. Jones HM, Parrott N, Jorga K, Lave T. A novel strategy for physiologically based predictions of human pharmacokinetics. Clin Pharmacokinet. 2006; 45:511–42. [PubMed: 16640456]
73. Rodgers T, Rowland M. Mechanistic approaches to volume of distribution predictions: understanding the processes. Pharm Res. 2007; 24:918–33. [PubMed: 17372687]
74. Jones HM, et al. Physiologically based pharmacokinetic modeling in drug discovery and development: a pharmaceutical industry perspective. Clin Pharmacol Ther. 2015; 97:247–62. [PubMed: 25670209]
75. Tomita Y, Maeda K, Sugiyama Y. Ethnic variability in the plasma exposures of OATP1B1 substrates such as HMG-CoA reductase inhibitors: a kinetic consideration of its mechanism. Clin Pharmacol Ther. 2013; 94:37–51. [PubMed: 23443754]
76. Vanstraelen K, et al. Posaconazole plasma exposure correlated to intestinal mucositis in allogeneic stem cell transplant patients. Eur J Clin Pharmacol. 2016; 72:953–63. [PubMed: 27066958]
77. Ke R, et al. Modelling clinical data shows active tissue concentration of daclatasvir is 10-fold lower than its plasma concentration. J Antimicrob Chemother. 2014; 69:724–7. [PubMed: 24169581]
78. Uchida Y, et al. Blood-brain barrier pharmacoproteomics-based reconstruction of the in vivo brain distribution of P-glycoprotein substrates in cynomolgus monkeys. J Pharmacol Exp Ther. 2014; 350:578–88. [PubMed: 24947467]
79. Huang H, et al. FABP1: A Novel Hepatic Endocannabinoid and Cannabinoid Binding Protein. Biochemistry. 2016; 55:5243–55. [PubMed: 27552286]
80. Edington CD, et al. Interconnected Microphysiological Systems for Quantitative Biology and Pharmacology Studies. Sci Rep. 2018; 8:4530. [PubMed: 29540740]
81. Mehrotra N, et al. Role of Quantitative Clinical Pharmacology in Pediatric Approval and Labeling. Drug Metab Dispos. 2016; 44:924–33. [PubMed: 27079249]
82. Zhang Z, Unadkat JD. Development of a Novel Maternal-Fetal Physiologically Based Pharmacokinetic Model II: Verification of the model for passive placental permeability drugs. Drug Metab Dispos. 2017; 45:939–46. [PubMed: 28049636]
83. Brouwer KL, et al. Human Ontogeny of Drug Transporters: Review and Recommendations of the Pediatric Transporter Working Group. Clin Pharmacol Ther. 2015; 98:266–87. [PubMed: 26088472]
84. Mooij MG, et al. Development of Human Membrane Transporters: Drug Disposition and Pharmacogenetics. Clin Pharmacokinet. 2016; 55:507–24. [PubMed: 26410689]
85. Peng KW, Bacon J, Zheng M, Guo Y, Wang MZ. Ethnic variability in the expression of hepatic drug transporters: absolute quantification by an optimized targeted quantitative proteomic approach. Drug Metab Dispos. 2015; 43:1045–55. [PubMed: 25926430]
86. Tsamandouras N, et al. Identification of the effect of multiple polymorphisms on the pharmacokinetics of simvastatin and simvastatin acid using a population-modeling approach. Clin Pharmacol Ther. 2014; 96:90–100. [PubMed: 24598718]
87. Toshimoto K, Tomoda Y, Chiba K, Sugiyama Y. Analysis of the Change in the Blood Concentration-Time Profile Caused by Complex Drug-Drug Interactions in the Liver Considering the Enterohepatic Circulation: Examining Whether the Inhibition Constants for Uptake, Metabolism, and Biliary Excretion Can be Recovered by the Analyses Using Physiologically Based Pharmacokinetic Modeling. J Pharm Sci. 2017; 106:2727–38. [PubMed: 28479365]
88. Zamek-Gliszczynski MJ, Chu X, Polli JW, Paine MF, Galetin A. Understanding the transport properties of metabolites: case studies and considerations for drug development. Drug Metab Dispos. 2014; 42:650–64. [PubMed: 24346835]
89. Culot M, et al. A simple method for assessing free brain/free plasma ratios using an in vitro model of the blood brain barrier. PLoS One. 2013; 8:e80634. [PubMed: 24312489]

90. Takano A, et al. Evaluation of in vivo P-glycoprotein function at the blood-brain barrier among MDR1 gene polymorphisms by using 11C-verapamil. J Nucl Med. 2006; 47:1427–33. [PubMed: 16954549]
91. Eyal S, et al. Regional P-glycoprotein activity and inhibition at the human blood-brain barrier as imaged by positron emission tomography. Clin Pharmacol Ther. 2010; 87:579–85. [PubMed: 20336065]
92. Liu L, et al. Modulation of P-glycoprotein at the Human Blood-Brain Barrier by Quinidine or Rifampin Treatment: A Positron Emission Tomography Imaging Study. Drug Metab Dispos. 2015; 43:1795–804. [PubMed: 26354948]
93. Deo AK, et al. Activity of P-Glycoprotein, a beta-Amyloid Transporter at the Blood-Brain Barrier, Is Compromised in Patients with Mild Alzheimer Disease. J Nucl Med. 2014; 55:1106–11. [PubMed: 24842892]
94. Bauer M, et al. Pilot PET Study to Assess the Functional Interplay Between ABCB1 and ABCG2 at the Human Blood-Brain Barrier. Clinical pharmacology and therapeutics. 2016; 100:131–41. [PubMed: 26940368]
95. Takashima T, et al. The involvement of organic anion transporting polypeptide in the hepatic uptake of telmisartan in rats: PET studies with [(1)(1)C]telmisartan. Mol Pharm. 2011; 8:1789–98. [PubMed: 21812443]
96. Takashima T, et al. Evaluation of breast cancer resistance protein function in hepatobiliary and renal excretion using PET with 11C-SC-62807. J Nucl Med. 2013; 54:267–76. [PubMed: 23287578]
97. Takashima T, et al. PET imaging-based evaluation of hepatobiliary transport in humans with (15R)-11C-TIC-Me. J Nucl Med. 2012; 53:741–8. [PubMed: 22499612]
98. Takano H, et al. Possible Role of Organic Cation Transporters in the Distribution of [(11)C]Sulpiride, a Dopamine D2 Receptor Antagonist. Journal of pharmaceutical sciences. 2017; 106:2558–65. [PubMed: 28499878]
99. Shingaki T, et al. Quantitative Evaluation of mMate1 Function Based on Minimally Invasive Measurement of Tissue Concentration Using PET with [(11)C]Metformin in Mouse. Pharm Res. 2015; 32:2538–47. [PubMed: 25715695]
100. Sundelin E, et al. Genetic Polymorphisms in Organic Cation Transporter 1 Attenuates Hepatic Metformin Exposure in Humans. Clin Pharmacol Ther. 2017; 102:841–8. [PubMed: 28380657]
101. Neyt S, et al. Synthesis, in vitro and in vivo small-animal SPECT evaluation of novel technetium labeled bile acid analogues to study (altered) hepatic transporter function. Nucl Med Biol. 2016; 43:642–9. [PubMed: 27513813]
102. Takahara N, et al. Drugs interacting with organic anion transporter-1 affect uptake of Tc-99m-mercaptoacetyl-triglycine (MAG3) in the human kidney: therapeutic drug interaction in Tc-99m-MAG3 diagnosis of renal function and possible application of Tc-99m-MAG3 for drug development. Nucl Med Biol. 2013; 40:643–50. [PubMed: 23618840]
103. Jamei M, et al. A mechanistic framework for in vitro-in vivo extrapolation of liver membrane transporters: prediction of drug-drug interaction between rosuvastatin and cyclosporine. Clin Pharmacokinet. 2014; 53:73–87. [PubMed: 23881596]
104. Yang K, et al. Systems pharmacology modeling of drug-induced hyperbilirubinemia: Differentiating hepatotoxicity and inhibition of enzymes/transporters. Clin Pharmacol Ther. 2017; 101:501–9. [PubMed: 28074467]
105. Li R, Ghosh A, Maurer TS, Kimoto E, Barton HA. Physiologically based pharmacokinetic prediction of telmisartan in human. Drug Metab Dispos. 2014; 42:1646–55. [PubMed: 25092714]
106. Gertz M, Tsamandouras N, Sall C, Houston JB, Galetin A. Reduced physiologically-based pharmacokinetic model of repaglinide: impact of OATP1B1 and CYP2C8 genotype and source of in vitro data on the prediction of drug-drug interaction risk. Pharm Res. 2014; 31:2367–82. [PubMed: 24623479]
107. Yamamoto Y, et al. Prediction of human CNS pharmacokinetics using a physiologically-based pharmacokinetic modeling approach. Eur J Pharm Sci. 2017; 112:168–79. [PubMed: 29133240]
108. Ibrutinib Clinical Pharmacology Review. 2013. https://wwwaccessdatafdagov/drugsatfda_docs/nda/2013/205552Orig1s000ClinPharmRpdf

109. Levonorgestrel Clinical Pharmacology Review. https://wwwaccessdatafdagov/drugsatfda_docs/nda/2013/203159Orig1s000ClinPharmRpdf

110. Edwards JE, et al. Modeling and Experimental Studies of Obeticholic Acid Exposure and the Impact of Cirrhosis Stage. Clin Transl Sci. 2016; 9:328–36. [PubMed: 27743502]

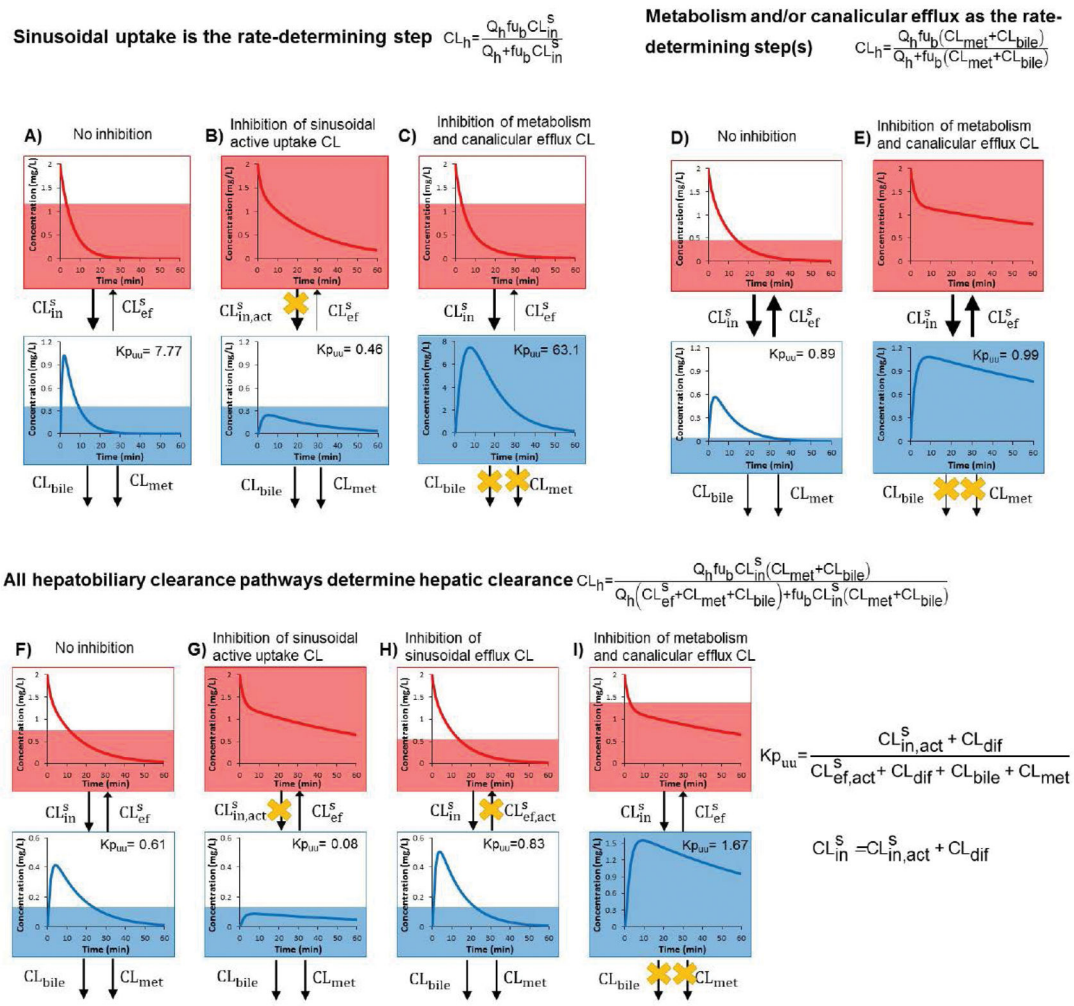

Figure 1.

The extended clearance model for hepatic disposition of a drug described by sinusoidal active influx ($CL^s_{in,act}$) and efflux clearances ($CL^s_{ef,act}$), passive diffusion (CL_{dif}), canalicular efflux (biliary) clearance (CL_{bile}), metabolic clearance (CL_{met}), hepatic blood flow, Q_h, and fraction unbound of the drug in the blood (fu_b). Total CL^s_{in} and CL^s_{ef} shown in governing equations include both active and passive processes (e.g., $CL^s_{in} = CL^s_{in,act} + CL_{dif}$). For all graphs, the red and blue lines represent the systemic and hepatic drug concentration-time profile, respectively. The blue and red shaded areas represent the relative systemic and hepatic drug AUC, respectively. **A–C)** CL^s_{in} is the rate determining step in the hepatic CL of a drug ($CL^s_{ef} \ll (CL_{met} + CL_{bile})$) thus creating a sink condition in the liver (e.g., rosuvastatin). When the aforementioned condition is met, the systemic AUC of the drug will increase when $CL^s_{in,act}$ is inhibited (**A** vs. **B**, top/red panels) but not when $CL_{met} + CL_{bile}$ is inhibited (**A** *vs.* **C**, top/red panels), even if there is significant elimination of the drug via metabolism or biliary efflux. In contrast, the hepatic AUC of the drug will not change when $CL^s_{in,act}$ is inhibited (**A** *vs.* **B**, bottom/blue panels) provided that the liver is the predominant or sole elimination organ but the hepatic drug concentration-time profile (e.g., C_{max} and T_{max}) will be altered. The hepatic AUC of the drug will increase when CL_{met} (or

CL_{bile}) is inhibited (**A** *vs.* **C**, bottom/blue panels). **D–E)** CL_{met} and/or CL_{bile} become the rate determining step in the hepatic CL of a drug when a drug can easily traverse the sinusoidal membrane (CL^{s}_{in} =CL^{s}_{ef} and much greater than CL_{met} + CL_{bile}, perfusion limited model). When this condition is met, the systemic and hepatic AUC of the drug will increase if either CL_{met} or CL_{bile} is inhibited (**D** *vs.* **E**). **F–I)** All hepatobiliary clearances affect hepatic CL of the drug when the drug is substrate of both enzymes and transporters but neither of the previous extreme conditions apply (e.g., repaglinide). Under this condition, inhibition of any of the hepatobiliary clearance will result in changes in the systemic AUC of the drug: increase due to $CL^{s}_{in,act}$, decrease due to $CL^{s}_{ef,act}$, and increase due to CL_{met} or CL_{bile} (**F** *vs.* **G**, **H**, **I** top/red panels, respectively). However, as long as the liver is the predominant elimination organ, the hepatic AUC of the drug will not change if $CL^{s}_{in,act}$ or $CL^{s}_{ef,act}$ are inhibited (**F** *vs.* **G** and **H**, bottom/blue panels, respectively). Hepatic AUC of the drug will increase when CL_{met} or CL_{bile} is inhibited (**F** *vs.* **I**, bottom/blue panels). The following values were used for simulation **A–C**: CL_{dif}= 0.1 L/min, $CL^{s}_{in,act}$ = 10 L/min, $CL^{s}_{ef,act}$ = 0 L/min, CL_{met} + CL_{bile} = 1.2 L/min, 95% inhibition of $CL^{s}_{in,act}$ or CL_{met} + CL_{bile} was simulated. **D–E**: CL_{dif}= 10 L/min, $CL^{s}_{in,act}$ = $CL^{s}_{ef,act}$ = 0.1 L/min (CL^{s}_{in} = CL^{s}_{ef}), CL_{met} + CL_{bile} = 1.2 L/min, 95% inhibition of CL_{met} + CL_{bile} was simulated. **F–I**: CL_{dif}= 0.1 L/min, $CL^{s}_{in,act}$ = 1 L/min, $CL^{s}_{ef,act}$ = 0.5 L/min, CL_{met} + CL_{bile} = 1.2 L/min, 95% inhibition of individual parameters was simulated. In all scenarios, liver is the main eliminating organ, Q_h was set arbitrarily at 1 L/min, and fu_b = $f_{u,liver}$ =1. Steady-state Kp_{uu} values calculated from individual parameters are shown. Figure is adapted and revised from Patilea-Vrana and Unadkat (Patilea-Vrana, G. & Unadkat, J.D. Transport vs. Metabolism: What Determines the Pharmacokinetics and Pharmacodynamics of Drugs? Insights From the Extended Clearance Model. Clin Pharmacol Ther 100, 413–8 [2016].).

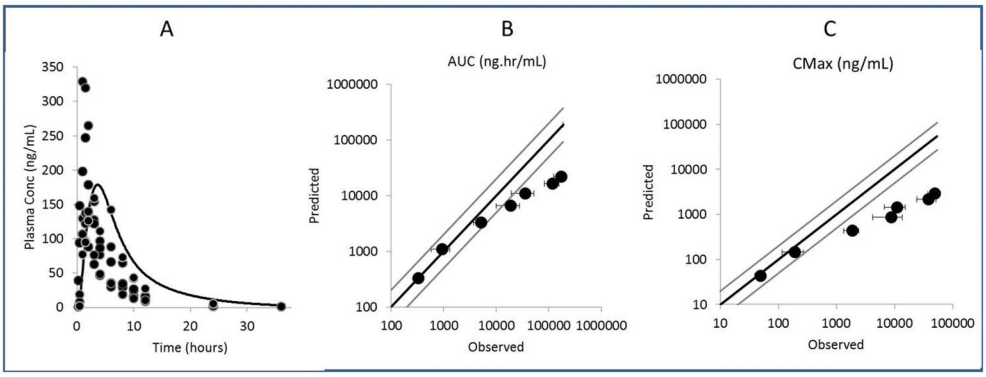

Figure 2.

(Upper) Simulated and individual observed plasma concentrations for an oral dose of 100 mg. (Lower) Predicted and Observed C_{max} and AUC at doses of 30 mg to 2000 mg.

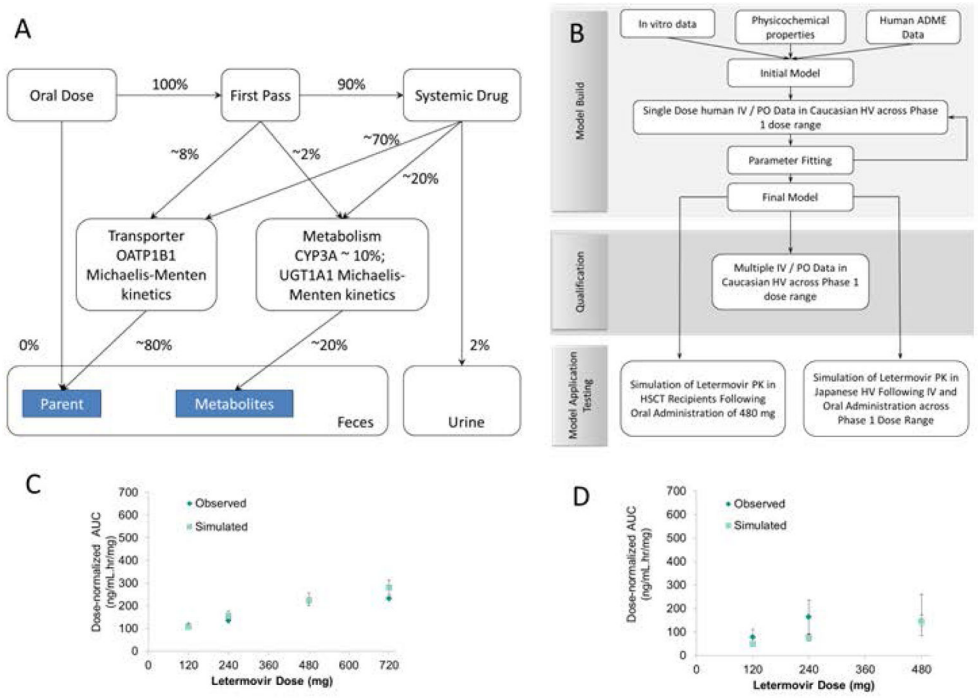

Figure 3.

A) A summary of the disposition characteristics of letermovir. **B)** The workflow of letermovir PBPK model development and the model qualification plan. An initial PBPK model was built in Simcyp® using a combination of physicochemical properties, preclinical data (*in vitro* and *in vivo*), and human ADME information of letermovir. In the next stage, the letermovir PBPK model was refined after the model parameters were optimized by plasma concentration-time profiles and PK data from Caucasian healthy volunteers (HV) receiving single IV and oral doses of letermovir at various dose levels in Phase 1 studies. Selected parameters, including the intrinsic clearance via oxidative metabolism and biliary excretion, Vmax and K_m parameters characterizing OATP1B-mediated transport into the liver, the unbound fraction in intracellular water, K_p scalar and first order oral absorption rates (ka) were optimized by the observed IV and oral healthy volunteer PK data. The final PBPK model was qualified based on PK and concentration-time profiles after multiple IV and oral doses of letermovir administered to Caucasian HV. Subsequently, the qualified letermovir PBPK model was applied to address the following questions for the development program: 1) explain mechanistically the difference in letermovir exposure observed in Caucasian and Japanese healthy subjects; 2) generate hypotheses that describe the exposure difference observed in Caucasian HV and hematopoietic stem cell transplant (HSCT) recipients after oral dosing. **C - D)** Observed and simulated systemic PK of letermovir in Caucasian healthy volunteers after single doses across the dose range of 120 to 720 mg IV (**C**) and 120 to 480 mg PO (**D**).

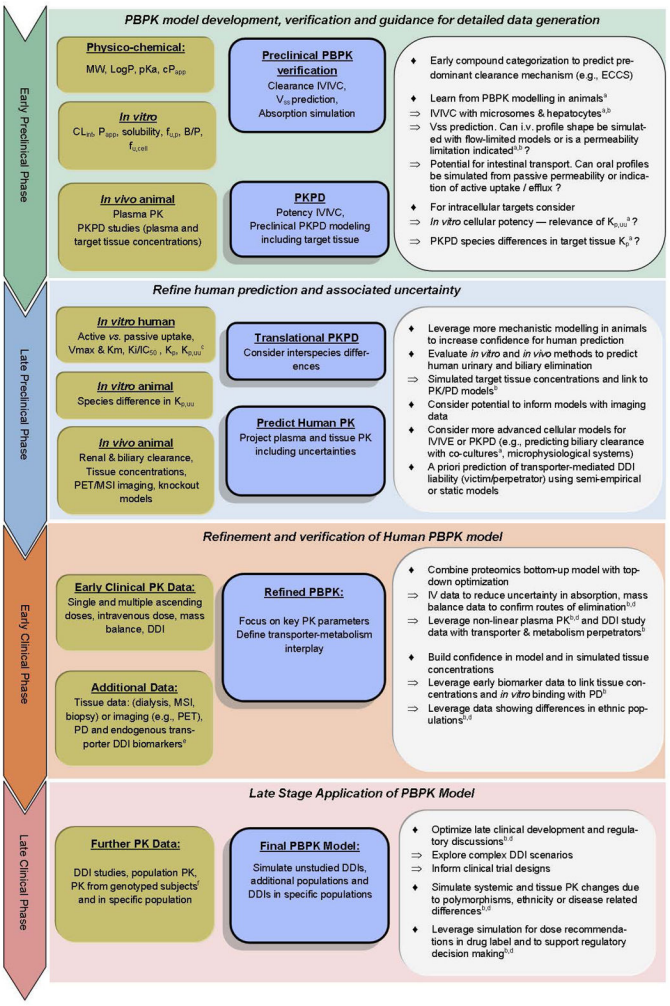

Figure 4.

Integrated workflow to illustrate *in vitro*, preclinical and clinical data generation and modeling considerations to identify, characterize and predict human pharmacokinetics in plasma and tissues for molecules where transport plays an important role.

[a]Case study 1, [b]Case study 3, [c]Table 1, [d]Case study 2

Table 1

experimental systems to determine *in vitro* K_{puu}

e equations developed for $K_{p,uu}$	Experimental systems	Assumptions	Advantages	Limitations	Number of Compounds tested
$\times f_{u,cell}$ (12, 15)	Transfected HEK293 cells & Suspended human hepatocytes	• Negligible CL_{int} • Steady-state reached • $f_{u,cell}$ is not influenced by cell homogenization	• Direct measurement of cellular drug binding • Agnostic towards the processes involved in binding	• Does not consider drug metabolism→ overestimate true $K_{p,uu}$ • Functional activity of efflux transporters were not confirmed • Mechanical cell homogenization not only disrupt the plasma membrane but also break cell organelles including intracellular membranes→ lower $f_{u,cell}$	18 (15) 30 (12)
$K_p \times \frac{f_{u,cell}}{f_{u,medium}}$ (14)	Suspended human & rat hepatocytes				6
$\times f_{u,liver}$ ($f_{u,cell}$) (13)	Sandwich-Cultured Hepatocytes & Liver Tissue	• $f_{u,cell}$ ($f_{u,liver}$) is not influenced by cell (tissue) homogenization • $f_{u,medium}$ = 1		• Organ-Specific • Cross-contamination among isolated cellular fractions. • Potential disruption of binding equilibrium between cellular compartments	3
$K_p \times \frac{f_{u,brain}(f_{u,slice})}{f_{u,plasma}}$ (89)	Brain tissue & Brain slice	• $f_{u,brain}$ ($f_{u,slice}$) is not influenced by tissue homogenization			30
$\frac{K_p(37°C)}{K_p(on\ ice)}$	Suspended human & rat hepatocytes	• Negligible CL_{int} • Steady-state reached • Active uptake is completely diminished on ice • $f_{u,liver}$ does not depend on the temperature	• Direct measurement of cellular drug binding • Agnostic towards the processes involved in binding	• Does not consider drug metabolism→ overestimate true $K_{p,uu}$ • Functional activity of efflux transporters were not confirmed • Potential artifacts on nonspecific binding and membrane fluidity and partitioning	3 (17) 15 (41)

e equations developed for $K_{p,uu}$	Experimental systems	Assumptions	Advantages	Limitations	Number of Compounds tested
$\times fu_{hep,logD}$ $_{gD} = -0.9161 - 0.2567 \times logD_{7.4}$	Suspended human hepatocytes	• Negligible CL_{int} • Steady-state reached • $f_{u,medium}$ =1	• Provides an early estimate of $f_{u,cell}$ in the absence of in vitro data	• Does not consider drug metabolism→ overestimate true $K_{p,uu}$ • Functional activity of efflux transporters were not confirmed • The association between intracellular unbound fraction and $LogD_{7.4}$ was based on 13 drugs, which are all anionic transporter substrates.	18
$1 + \frac{CL^s_{in,act}}{CL_{dif}} CL^s_{in,act} = \frac{V_{max}}{K_m}$	Suspended rat hepatocytes	• Negligible $CL_{bile} + CL_{met} \& CL^s_{ef,act}$ • $CL^s_{in,act}$ equals to the initial uptake rate • Passive influx and efflux diffusion permeation equal to CL_{dif}	• Mechanistically informative	• Does not consider drug metabolism and active efflux→overestimate true $K_{p,uu}$ • $CL^s_{in,act}$ is calculated based on the initial uptake, which may include the transport mediated by both facilitated diffusion transporters and active transporters→ overestimate true $K_{p,uu}$ • Passive influx diffusion permeation might be smaller than passive efflux diffusion permeation in the case of anions→ overestimate true $K_{p,uu}$	16

e equations developed for $K_{p,uu}$	Experimental systems	Assumptions	Advantages	Limitations	Number of Compounds tested
$\frac{CL^{s}_{in,act}+CL_{dif}}{CL^{s}_{ef,act}+CL_{dif}+CL_{bile}+CL_{met}}$		• Negligible $CL^{s}_{ef,act}$ • Passive influx and efflux diffusion permeation equal to CL_{dif} (15)	• Mechanistically informative	• All individual *in vitro* parameters and the methods to measure these parameters are not fully validated with *in vivo* data.	18 (15)
		• Negligible $CL_{bile}+CL_{met}$&$CL^{s}_{ef,act}$(17)			3 (17)

clearance of unbound drugs for influx across the sinusoidal membrane via transporter(s); $CL^{s}_{ef,act}$: membrane permeation clearance of unbound drugs for efflux across porter(s); CL_{dif}: membrane permeation clearance of unbound drugs for influx or efflux across the sinusoidal membrane by passive diffusion; CL_{bile}: hepatic intrinsic iliary excretion of unchanged drugs; CL_{met}: hepatic intrinsic clearance (of unbound drugs) for metabolism of unchanged drugs; K_p, the membrane partition coefficient, tocyte-to-medium total drug concentration ratio; $K_{p,uu}$, hepatocyte-to-medium partition coefficient for unbound drug concentration; $f_{u,liver}$: liver tissue protein unbound nd drug in cell; $f_{u,hep}$, fraction of unbound drug in hepatocyte incubations; $f_{u,medium}$, fraction of unbound drug in medium; V_{max}, maximum transport or metabolic CM, extended clearance model.

Table 2

Selected examples of imaging studies used to evaluate transporter-mediated distribution and drug-drug interactions *in vivo* in preclinical species and humans

Imaging Modality	Imaging Ligand	Species	Transporters	Tissue	Objectives	Reference
PET	^{11}C-verapamil	Human	P-gp	BBB	**1** Determine if P-gp functionality at the human BBB can affect the brain distribution of a model P-gp substrates, verapamil **2** Assess the magnitude of DDI at the human BBB using a potent inhibitor of P-gp, cyclosporine A (CsA), and a model P-gp substrate, verapamil	(6)
	^{11}C-verapamil	Human	P-gp	BBB	Determine whether the P-gp function at the human BBB is different between the haplotypes (1236TT, 2677TT, 3435TT vs. 1236CC, 2677GG, 3435CC) of the MDR1 gene	(90)
	^{11}C-verapamil	Human	P-gp	BBB	Determine regional BBB P-gp activity	(91)
	^{11}C-verapamil	Human	P-gp	BBB	**1** Determine if quinidine, at therapeutic doses, is a more potent inhibitor of P-gp at the human BBB than CsA **2** Assess whether rifampin, a potent intestinal P-gp inducer, can induce P-gp at the human BBB	(92)
	^{11}C-verapamil	Human	P-gp	BBB	**3** Determine if P-gp function at the BBB is reduced in Alzheimer's disease	(93)
	^{11}C-elacridar and ^{11}C-tariquidar	Human	P-gp/BCRP	BBB	Determine if ^{11}C-elacridar or ^{11}C-tariquidar can be used to interrogate BCRP activity at the BBB	(94)
	^{11}C-telmisartan	Rat	Oatp/Mrp2	Liver, intestine	Investigate hepatic uptake and biliary excretion of telmisartan +/− rifampicin over dose range	(95)
	^{11}C-celecoxib carboxylic acid (SC-62807)	Mice	Oatp/Bcrp	Liver, intestine	Investigate feasibility of SC-62807 to evaluate BCRP activity in preclinical species and humans	(96)

Imaging Modality	Imaging Ligand	Species	Transporters	Tissue	Objectives	Reference
	(15*R*)-16-m-[^{11}C]tolyl-17,18,19,20-tetranorisocarbacyclin methyl ester (^{11}C-TIC Me)	Human	OATP/MRP2	Liver, kidneys, bile	Investigate use of ^{11}C-TIC Me to detect changes in OATP function in human hepatobiliary transport in the presence of rifampicin	(97)
	^{11}C-sulpiride	Mice, Human	Oct1/2, Mates OCT1, OCT2, MATE1 and MATE2-K	Liver, kidneys	Determine the tissue distribution of ^{11}C-sulpiride in mice and in human to evaluate OCT and MATE activity *in vivo*	(98)
	^{11}C-metformin	Mice	mMate1	Liver, kidneys	Evaluate the function of MATEs and investigate the impact of pyrimethamine on hepatic and renal exposure of metformin relative to systemic exposure	(99)
	^{11}C-metformin	Human	OCT1	Liver, intestine, muscle, kidneys	Investigate the impact of *SLC22A1* allelic variants with reduced OCT1 activity on metformin hepatic exposure relative to systemic exposure	(100)
γ S/SPECT	^{99m}Tc–mebrofenin (MEB)	Human	OATP1B1, OATP1B3, MRP2	Liver	**1** Elucidate the sites and impact (systemic and hepatic exposure) of the hepatobiliary transport DDI between ritonavir and ^{99m}Tc–mebrofenin in humans **2** Substantiate predictions from modeling and simulation of clinical data that ritonavir inhibited OATP-mediated hepatic uptake but not MRP2-mediated biliary excretion of ^{99m}Tc–mebrofenin using sandwich-cultured human hepatocytes	(56)
	^{99m}Tc–mebrofenin	Mice	Oatp1a/1b, Mrp2	Liver	Elucidate the sites and impact (systemic and hepatic exposure) of the hepatobiliary transport DDI between rifampicin and ^{99m}Tc–mebrofenin in mice	(101)
	^{99m}Tc-DTPA-chenodeoxycholic acid (CDCA) and ^{99m}Tc-DTPA-cholic acid (CA)	Mice	Oatp1a/1b, Mrp2	Liver	Elucidate the sites and impact (systemic and hepatic exposure) of the hepatobiliary transport DDI between rifampicin and ^{99m}Tc–DTPA-CDCA and ^{99m}Tc–DTPA-CA in mice	(101)
	^{99m}Tc - mercaptoacetyl-triglycine (MAG3 - used to diagnose function of the kidneys)	Human	OAT1 and OAT3	Kidneys	Investigate whether treatment with OAT inhibitors (probenecid, PAH) may affect the renal uptake of ^{99m}Tc - MAG3	(102)
Contrast-Enhanced MRI	Gadolinium-ethoxybenzyl-diethylenetriame-pentaacetic acid (Gd-EOOB-DTPA; Gadoxetate)	Rat		Liver	**1** Estimate the intracellular concentration of gadoxetate in rat liver	(58)

Imaging Modality	Imaging Ligand	Species	Transporters	Tissue	Objectives		Reference
					2	Quantify the hepatic uptake and excretion of gadoxetate in rats, and the impact of a biliary transport inhibitor	
	Gadoxetate	Human	OATP1B1, OATP1B3	Liver	1	Determine if OATP1B1 and OATP1B3 genetic polymorphisms influence gadoxetate uptake *in vitro*	(59)
					2	Assess whether functionally relevant polymorphisms are confounders for liver enhancement by gadoxetate in healthy humans	

Table 3

Published and regulatory examples of PBPK and PBPK-PD modeling of systemic and tissue exposure as a result of transporter DDIs and/or organ impairment

Drug	Specificity/ novelty of the PBPK model	Step-wise model verification	Key applications	Verification of simulated tissue exposure	Reference
Literature Examples					
Simvastatin acid and lactone	• Reduced PBPK model - mechanistic description of liver (efficacy/DDI), intestine (DDI) and muscle (safety) compartments • Population PBPK model – Clinical data and maximum a posteriori method used for estimation of missing model parameters (e.g., $CL^{s}_{in,act}$ for acid) • Acid-lactone interconversion at multiple sites implemented	• Independent clinical data for the acid and lactone form • Prediction of *SLCO1B1* c. 521T>C effect on systemic exposure of the acid/lactone • Prediction of CYP3A4 DDIs (reversible and irreversible perpetrators with inhibitory metabolites)[a]	Prediction of changes in the acid/ lactone liver and muscle exposure in: **i.** *SLCO1B1* c.521T>C subjects **ii.** CYP3A4 DDIs Model predicted disconnect between changes in systemic and liver exposure as a result of *SLCO1B1* c. 521T>C	Indirect verification based on PD data (liver) and toxicity/safety data (muscle) reported in *SLCO1B1* c. 521T>C subjects and CYP3A4 DDIs	(3)
Rosuvastatin	• Based on the PBPK model described and verified for cyclosporine DDI in (103) • Optimization of OATP1B1-mediated uptake clearance by clinical data from *SLCO1B1* c. 521T>C subjects • PBPK-PD model, simulated rosuvastatin liver or plasma concentrations evaluated as input in the PD model	• Prediction of SLCO1B1 c. 521T>C effect on rosuvastatin PD effect and associated inter-subject variability	Model predicted disconnect between changes in systemic and liver exposure as a result of *SLCO1B1* c. 521T>C Use of PBPK simulated liver concentration to drive the PD response predicted correctly minor effect of *SLCO1B1* c.521T>C on cholesterol synthesis	Indirect verification based on PD marker data (mevalonic acid) in *SLCO1B1* c. 521T>C	(62)
Bilirubin	• Update of the DILIsym model • Incorporates OATP1B1/1B3 uptake, biliary (MRP2), basolateral efflux (MRP3) and UGT metabolism of bilirubin • Simulated total and % conjugated bilirubin	• Clinical data in subjects with inherited metabolism/transport disorders (GS, RS, DJS)[b] • Prediction of the effect of indinavir (also in GS subjects), nelfinavir and investigational drug on total bilirubin	Differentiation between hepatotoxicity and transporter DDIs as causes of drug induced hyperbilirubinemia Proposed for prospective prediction of increased bilirubin by drug candidates	Preclinical studies in rat	(104)

Drug	Specificity/ novelty of the PBPK model	Step-wise model verification	Key applications	Verification of simulated tissue exposure	Reference
Telmisartan	• IVIVE of $CL^{s}_{in,act}$, CL_{bile} and CL_{met} for the parent and glucuronide using ESFs obtained from multiple OATP drugs • Kp values predicted by Rodgers & Rowland method (73) were optimized using PET data • Model extended to account for enterohepatic recirculation	• Verification of the model against i.v. infusion and oral data	Development of the parent-metabolite model Prediction of parent/glucuronide concentrations in the liver tissue and residual liver bile – calibration with PET data Use of PET Kp improved the prediction of Vd (mostly related to corrected muscle Kp estimate)	ESF for glucuronide CL_{bile} was estimated using the total amount of telmisartan and telmisartan glucuronide in the liver observed in the PET study	(105)
Repaglinide	• Reduced PBPK model - mechanistic description of liver compartment • Population PBPK model – clinical data used for estimation of $CL^{s}_{in,act}$ in subjects with different *SLCO1B1* (521T>C) polymorphisms • Sensitivity analysis to investigate impact of CL_{met} and CL_{dif} on the estimation of $CL^{s}_{in,act}$ from plasma data (reverse translation) • Impact of parameter uncertainty on liver exposure and DDI prediction	• Prediction of *SLCO1B1* c. 521T>C effect on repaglinide systemic exposure • Simulation of inter-subject variability in repaglinide AUC and C_{max} • Uncertainty in CL_{met} and CL_{dif} results in >50-fold difference in IVIVE empirical scalars for repaglinide $CL^{s}_{in,act}$	Model used to simulate the effect of combined CYP2C8*3 and SLCO1B1 c.521T>C on repaglinide plasma exposure Power calculations to guide prospective DDI/ pharmacogenetics studies Illustrates that multiple solutions for optimized $CL^{s}_{in,act}$ can recapitulate systemic exposure, but result in different simulated liver concentrations and liver	No tissue data available Predicted successfully inter-subject variability in repaglinide exposure	(106)
Acetaminophen Oxycodone Morphine Phenytoin	• Brain model consists of nine compartments, plasma, brain, microvessels, ECF, ICF, lysosomes and 3 CSF compartments • Contribution of active transporters scaled based on differences in expression in both species	Verified rat model scaled by replacing physiological parameters to predict human	Understanding of effect of pathophysiological changes on drug distribution in the brain Enables the prediction of CNS target-site concentrations in humans	Human simulations compared to ECF and/or CSF data	(107)
Digoxin	• Mechanistic kidney model (part of full PBPK model), regional differences considered • OATP4C1 $CL_{int,T}$ estimated using digoxin clinical CL_R data (214 subjects)	• Independent clinical studies – plasma and urinary-excretion time data	Successful prediction of renal clearance in patients with: **i.** moderate and severe renal impairment **ii.** elderly	No tissue data available Assumed RI mechanism of active secretion - implications for nephrotoxicity and renal	(66)

Drug	Specificity/ novelty of the PBPK model	Step-wise model verification	Key applications	Verification of simulated tissue exposure	Reference
	• Different mechanisms of altered active secretion in RI patients investigated in the model: **i.** reduced transporter expression **ii.** reduced proximal tubule cellularity[c] (4.5 to 9-fold reduction required for severe RI) **iii.** as above but proportional to GFR reduction		Assumed mechanisms of altered active secretion in RI resulted in: • Comparable predicted systemic exposure and CL_R • Differences in simulated maximal proximal tubule concentrations	transporter-mediated DDIs	
Cidofovir Oseltamivir carboxylate Cefuroxime	• Mechanistic kidney model (part of full PBPK model), regional differences considered • $CL_{int,T}$ optimization in a stepwise manner: OAT-mediated using plasma data[d], efflux $CL_{int,T}$ based on urine accumulation data • Changes in active secretion in RI patients implemented in the model as reduced proximal tubule cellularity[c] (>10-fold reduction required for severe)	• Independent clinical studies • Prediction of renal DDI with probenecid	Prediction of renal clearance in patients with severe renal impairment (effect on proximal tubule concentrations not explored) Simulation of cidofovir nephrotoxicity and estimation of probenecid *in vivo* Ki	Indirect verification based on cidofovir nephrotoxicity data	(64)
Adefovir Avibactam Entecavir Famotidine Ganciclovir Oseltamivir carboxylate Sitagliptin	• Mechanistic kidney model (part of full PBPK), regional differences considered • Nonrenal CL back-calculated from systemic clearance and CL_r and assigned as undefined CL_H • OAT-mediated $CL_{int,T}$ obtained by parameter estimation using plasma data after i.v. administration • Different mechanisms of altered active secretion in CKD investigated: **i.** reduced proximal tubule cellularity[c]	• Verification of the base model against data in healthy subjects (oral)	Prediction of changes in systemic exposure and renal clearance in patients with moderate and severe renal impairment Most predicted AUCR and CLrR within 1.5-fold of the observed data with the exception of adefovir (>65% of predicted data within 1.25-fold) Effect of RI mechanism(s) on proximal tubule concentrations not investigated	No tissue data available	(65)

Drug	Specificity/ novelty of the PBPK model	Step-wise model verification	Key applications	Verification of simulated tissue exposure	Reference
	proportional to reduction in GFR **ii.** inhibition of OATs by uremic solutes implemented by reducing OAT RAF/REF in the CKD model • Nonrenal CL reduced by 31% and 36% for moderate and severe CKD[e]				
Regulatory Examples					
Ibrutinib	• Combination of *in vitro*, physicochemical, and clinical data • Fraction absorbed derived from clinical studies, $fu_{,gut}$ from sensitivity analysis to observed PK data, and CYP3A contribution to overall clearance verified by DDI studies • Used software's Advanced Dissolution, Absorption, Metabolism (ADAM) model to predict ibrutinib exposure in different segments of the GI tract to determine the potential for P-gp inhibition	• Prediction of CYP3A DDIs (inhibition and induction)	Simulation of luminal drug concentration-time profiles in GI segments predicted fast absorption of ibrutinib Staggering of ibrutinib dose and an oral P-gp substrate by at least 2.5 h could minimize potential for a P-gp interaction (i.e., avoid concomitant administration of P-gp substrate during the absorption phase of ibrutinib)	No tissue data available Indirect evidence: no clinically relevant DDI between ibrutinib and P-gp substrates have been reported to date	(108)
Levonorgestrel (LNG, an IUD)	• Combination of physicochemical properties, binding to SHBG (sex hormone binding globulin), *in vitro* release kinetics of LNG, and clinical PK studies to fit hepatic clearance • Assumed SHBG levels and variance in post-menarche population is comparable to those observed in adults • Incorporated a uterus model (myometrium, endometrium, cavity) with physiological parameters derived from literature	• Independent clinical studies	Used to predict plasma PK of LNG in adolescent females Cmax and AUC did not differ in females between 15–18 years to a clinically relevant extent (difference of median values < 10%). Median Cmax and AUC increased on average maximally by 60% in 10 year old female compared to adult females	Population PK analysis of Phase 3 study in adolescent females (12–18 years) showed that mean LNG serum concentrations were slightly higher (~10%) in adolescent females than in adult females	(109)

Drug	Specificity/ novelty of the PBPK model	Step-wise model verification	Key applications	Verification of simulated tissue exposure	Reference
	• Adult model scaled to post-menarche female adolescents by incorporating age-dependent changes in anatomy and physiology				
Both					
Simeprevir (OATP DDI)	• Nonlinearity in simeprevir PK at therapeutic doses • Combination of IVIVE of *in vitro* data (OATP1B1, 1B3 V_{max}, K_m) with optimization of parameters using clinical data (CYP3A4 V_{max} and K_m and $f_{u,IW}$)[f]	• Prediction of OATP DDI (multiple doses of cyclosporine)[a] • Prediction of CYP3A4 DDIs (inhibition and induction)[a] • Prediction of OATP and CYP3A4 combined DDIs (multiple doses of Rifampin)	Simulation of DDI risk for untested clinical interactions with a range of moderate and strong CYP3A4 inhibitors and rifampicin sd (OATP) Included in regulatory submissions to FDA and EMA Moderate or strong CYP3A inhibitors and strong OATP inhibitors are not recommended to be given concomitantly with simeprevir	*In vivo* preclinical studies used to support extensive liver accumulation	(69)
Simeprevir	• Modification of system parameters associated with hepatic impairment and hepatitis C virus (HCV) infection - reduced CYP3A4 expression, liver volume, hepatic blood flow • Modification of system parameters associated with ethnic differences (Chinese, Japanese) - reduced CYP3A4 expression, reduced liver volume	• Based on model described in (69) but applied to different populations. (see above) • Prediction of plasma exposure in Caucasian, Chinese and Japanese HCV-infected subjects	Simulation of simeprevir liver concentrations in HCV subjects with different ethnicity Translation of DDI risk from healthy to HCV-infected patients Simulated liver concentrations in Chinese and Japanese subjects with HCV (100 mg QD) were comparable with Caucasian HCV subjects (150 mg QD) No dose adjustment recommended based on ethnicity, but post marketing requirement issued to assess safety signals in HCV patients of East Asian ancestry	No data available to confirm simulated differences in simeprevir liver exposure	(70)
Obeticholic acid (OCA)	• PBPK model for OCA and conjugate metabolites • Modification of system parameters associated with hepatic impairment - either fixed (liver volume, Q_H) or estimated (hepatic uptake in HI) using plasma data for parent and metabolites in HI	• External clinical dataset in healthy and HI subjects	Simulation of systemic and liver profiles in severe HI (predicted 13- and 2-fold increase, respectively compared to healthy subjects) Included in regulatory submission to FDA Additional simulations of OCA PK in plasma and liver under different dosing schedules in healthy and HI requested by FDA. Final dose adjustment recommendation based on simulated plasma exposure	Indirect evidence: Severe liver injury and death reported in patients with moderate / severe HI who took OCA more frequently than recommended Healthcare providers urged to adhere to FDA's approved dosing regimen	(1, 110)

Drug	Specificity/ novelty of the PBPK model	Step-wise model verification	Key applications	Verification of simulated tissue exposure	Reference
				of OCA in patients with HI	

[a] Combination of the victim drug model with a qualified perpetrator PBPK model

[b] Gilbert's Syndrome (GS), Rotor syndrome (RS) and Dubin-Johnson Syndrome (DJS)

[c] System parameter – PTCPGK

[d] Data from three dose levels used for cidofovir and cefuroxime $CL_{int,T}$

[e] Same reduction factor applied for all drugs due to lack of data on pathway specific effects of CKD. Important for improved prediction of AUC for drugs with high nonrenal CL (entecavir)

[f] Biliary CL set based on mass balance data - simeprevir